

## MIT Open Access Articles

*Solutions of the stream power equation and application to the evolution of river longitudinal profiles*

The MIT Faculty has made this article openly available. **Please share** how this access benefits you. Your story matters.

**Citation:** Royden, Leigh, and J. Taylor Perron. "Solutions of the Stream Power Equation and Application to the Evolution of River Longitudinal Profiles." *Journal of Geophysical Research: Earth Surface* 118, no. 2 (June 2013): 497–518. Copyright © 2013 American Geophysical Union

**As Published:** <http://dx.doi.org/10.1002/jgrf.20031>

**Publisher:** American Geophysical Union (AGU)

**Persistent URL:** <http://hdl.handle.net/1721.1/85608>

**Version:** Final published version: final published article, as it appeared in a journal, conference proceedings, or other formally published context

**Terms of Use:** Article is made available in accordance with the publisher's policy and may be subject to US copyright law. Please refer to the publisher's site for terms of use.



# Solutions of the stream power equation and application to the evolution of river longitudinal profiles

Leigh Royden<sup>1</sup> and J. Taylor Perron<sup>1</sup>

Received 14 May 2012; revised 23 December 2012; accepted 7 January 2013; published 2 May 2013.

[1] Erosion by bedrock river channels is commonly modeled with the stream power equation. We present a two-part approach to solving this nonlinear equation analytically and explore the implications for evolving river profiles. First, a method for non-dimensionalizing the stream power equation transforms river profiles in steady state with respect to uniform uplift into a straight line in dimensionless distance-elevation space. Second, a method that tracks the upstream migration of slope patches, which are mathematical entities that carry information about downstream river states, provides a basis for constructing analytical solutions. Slope patch analysis explains why the transient morphology of dimensionless river profiles differs fundamentally if the exponent on channel slope,  $n$ , is less than or greater than one and why only concave-up migrating knickpoints persist when  $n < 1$ , whereas only concave-down migrating knickpoints persist when  $n > 1$ . At migrating knickpoints, slope patches and the information they carry are lost, a phenomenon that fundamentally limits the potential for reconstructing tectonic histories from bedrock river profiles. Stationary knickpoints, which can arise from spatially varying uplift rates, differ from migrating knickpoints in that slope patches and the information they carry are not lost. Counterparts to migrating knickpoints, called “stretch zones,” are created when closely spaced slope patches spread to form smooth curves in distance-elevation space. These theoretical results are illustrated with examples from the California King Range and the Central Apennines.

**Citation:** Royden, L., and J. Taylor Perron (2013), Solutions of the stream power equation and application to the evolution of river longitudinal profiles, *J. Geophys. Res. Earth Surf.*, 118, 497–518, doi:10.1002/jgrf.20031.

## 1. Introduction

[2] Tectonics and landscape evolution are inextricably linked in regions that have experienced recent deformation. Erosion rates, drainage network geometry, longitudinal river elevation profiles, and topography all reflect the interaction between surface uplift rate and the dynamics of river incision. A complete theory of coupled tectonic deformation and river incision would provide a means of translating among uplift rates, incision rates, and the geometry of river profiles, revealing information about local and regional uplift histories and hence about the underlying tectonic history. Quantifying the connection between uplift and river incision requires an understanding of both the tectonic processes that produce uplift and the erosional response to uplift.

[3] In this paper, we improve the quantitative understanding of this connection for fluvial systems that are dominated by bedrock channel incision. The evolution of bedrock river systems depends nonlinearly on topography and its spatial derivatives. Except in cases of steady state river systems, where incision and uplift rates are exactly balanced, the

nonlinear dynamics of these erosional systems has made it difficult to derive analytical solutions. The current understanding of transient bedrock river incision is therefore based almost entirely on numerical solutions. Here we obtain analytical solutions to the equations that govern bedrock river incision in order to examine the transient response of river systems to changes in uplift rate and precipitation and to events like river capture.

[4] We begin by briefly reviewing the most widely used model for bedrock river incision, the stream power model, and propose a non-dimensional change of variables that makes transient analytical solutions tractable and highlights deviations from steady state. We then present transient analytical solutions for simplified cases such as uplift rates that are constant in space and time, as well as for more complicated scenarios in which uplift rates vary in space and time. These analytical solutions highlight fundamental properties of evolving river profiles that may not be apparent in numerical solutions, including how information about past states of the river profile can be destroyed and how new topographic information can be created in the middle of the profile in addition to that at the downstream boundary. We illustrate the application of the non-dimensionalization and the analytical solutions to landscapes with documented examples of steady state and transient river profiles.

## 2. Dynamics of Bedrock River Incision

[5] The rate of bedrock river incision is generally assumed to be proportional to the shear stress [Howard and Kerby, 1983]

<sup>1</sup>Department of Earth, Atmospheric and Planetary Sciences, Massachusetts Institute of Technology, Cambridge, Massachusetts, USA.

Corresponding author: L. Royden, Department of Earth, Atmospheric and Planetary Sciences, Massachusetts Institute of Technology, Cambridge, MA 02139, USA. (lroyden@mit.edu)

©2013. American Geophysical Union. All Rights Reserved.  
2169-9003/13/10.1002/jgrf.20031

or the rate of energy expenditure [Seidl and Dietrich, 1992] related to flow over the river bed, raised to some power. The resulting family of models is referred to collectively as the stream power model. The shear stress or rate of energy expenditure is in turn proportional to the longitudinal river gradient, with a dependence that is usually parameterized through expressions for steady, uniform flow [Howard and Kerby, 1983; Howard, 1994]. Combining the stream power incision model with a large-scale mass conservation equation yields a partial differential equation that relates the change in elevation of the river bed with time to the uplift rate of the underlying rocks and the gradient of the river [e.g., Howard, 1994; Howard et al., 1994; Whipple and Tucker, 1999]:

$$\frac{\partial h}{\partial t} = u(x, t) - q(x, t) \left| \frac{\partial h}{\partial x} \right|^n \quad (1)$$

where  $h(x, t)$  is elevation of the river bed;  $u(x, t)$  is the rate of rock uplift;  $q(x, t)$  is a combined measure of the erodibility of bedrock, channel geometry, and the volume rate of flow, as defined below;  $x$  is horizontal distance measured along the river;  $t$  is time; and  $n$  is the exponent that governs the dependence of erosion rate on slope (Table 1).

[6] Considerable effort has been devoted to determining the value of the exponent  $n$  and the form of the function  $q$ . The value of  $n$  for a given river is usually not known a priori. Theoretical analyses [Howard and Kerby, 1983; Howard, 1994; Whipple, 2004] and field observations [Howard and Kerby, 1983; Seidl and Dietrich, 1992; Seidl et al., 1994; Rosenbloom and Anderson, 1994; Stock and Montgomery, 1999; Whipple et al., 2000; van der Beek and Bishop, 2003] have suggested that  $n$  typically lies between  $\frac{2}{3}$  and  $\frac{5}{3}$ . More recently, studies have suggested that the combination of an erosion threshold (that is, a critical stream power or shear stress that must be exceeded for erosion to occur) and a distribution of flow events over time may result in long-term effective values of  $n$  that exceed 2 [Snyder et al., 2003; Tucker, 2004; Lague et al., 2005; DiBiase and Whipple, 2011]. The value of  $n$ , particularly whether it is greater than or less than one, can significantly influence the evolution of river profiles [Whipple and Tucker, 1999; Tucker and Whipple, 2002], a phenomenon that we explore further in this paper. We do not assume any particular value for  $n$  in our theoretical analysis, but we subsequently offer several examples that illustrate the effects of this parameter.

[7] The function  $q$  depends on the volume rate of flow within the river, the channel roughness and cross-sectional geometry, the mechanical properties of the bedrock, and potentially the flux and character of sediment in the channel. If precipitation is uniform over the entire region of interest, then the volume rate of flow is proportional to the product of drainage area and effective precipitation rate, and the function  $q$  takes the form

$$q(x, t) = r(x)[A(x)p(t)]^m \quad (2)$$

where  $r(x)$  represents the lithologic and process control on erodibility,  $A(x)$  is drainage area,  $p(t)$  is effective precipitation rate averaged over the drainage area, and  $m$  is an exponent that relates erosion rate to volume rate of flow. Here in order to avoid the introduction of many additional variables, effective precipitation rate is assumed to incorporate the effects of evapotranspiration and groundwater losses. If precipitation rate is spatially variable or drainage area changes with time, then  $A$  and  $p$  can be redefined accordingly, such that  $A(x)$  describes the spatially variable component of both drainage area and precipitation rate, and  $p(t)$  describes the time-varying component of both drainage area and precipitation rate. For the purposes of our analysis, the most important characteristic of equation (2) is that  $q$  must be expressed as a product of functions that depend only on  $x$  and functions that depend only on  $t$ .

[8] The simplest version of the stream power model reduces channel incision rate to a dependence on drainage area and slope, typically with a constant coefficient. Equation (2) represents a more general formulation in which the function  $r(x)$  is assumed to incorporate the effects of spatially variable channel geometry and roughness, bedrock mechanical properties, and sediment load. Numerous studies have noted the potential importance of these and other factors and have suggested modifications to the conventional stream power model. Three proposed modifications are especially notable due to the empirical support for their influence on channel incision rates in some scenarios [Tucker and Hancock, 2010]. First, sediment can influence the channel incision rate both by protecting the bed from erosion [Beaumont et al., 1992] and by causing erosion through impacts and abrasion during transport [Sklar and Dietrich, 1998], two competing effects that have led to the suggestion that incision rates will be fastest at intermediate

**Table 1.** Variables Used in the Text

Variable	Units	Dimensionless Variable	Description or Comment
$h$	L	$\lambda$	Elevation
$h_o$	L		Reference elevation
$x$	L	$\chi$	Horizontal position
$u$	$L T^{-1}$	$v$	Uplift rate
$t$	T	$\tau$	Time
$A$	$L^2$		Upstream drainage area
$A_o$	$L^2$		Reference upstream drainage area
$r$	$L^{1-3m} T^{m-1}$		Erodibility (lithologic)
$r_o$	$L^{1-3m} T^{m-1}$		Reference erodibility (lithologic)
$p$	$L T^{-1}$		Precipitation
$p_o$	$L T^{-1}$		Reference precipitation
$q$	$L T^{-1}$	$\sigma$	Composite erodibility term
			Slope

sediment flux [Sklar and Dietrich, 2001, 2004, 2008; Turowski *et al.*, 2007]. Second, mechanically based models for channel width have been proposed as alternatives to empirical scalings with water discharge or drainage area [Finnegan *et al.*, 2005, 2007; Turowski *et al.*, 2009; Nelson and Seminara, 2011]. Third, the combination of a distribution of flow events over time and a threshold for sediment entrainment or erosion can influence the apparent erodibility [Snyder *et al.*, 2003; Tucker, 2004; Lague *et al.*, 2005; DiBiase and Whipple, 2011].

[9] Rather than attempting to treat these factors directly, we use the flexible formulation in equation (2), which assumes that spatially variable effects on erodibility can be described with the function  $r$ . Equation (2) can be reduced to the conventional form of the stream power model by treating precipitation rate and erodibility as constants. Our formulation is general, in the sense that factors beyond those mentioned here can be included in  $q$  and handled in the manner shown below.

### 3. Previous Analytical Studies

[10] Pioneering theoretical work on the transient development of stream profiles was described in a series of mathematical papers in the 1970s by Luke [1972, 1974, 1976]. Luke used the method of characteristics to describe the evolution of topographic profiles and surfaces in response to an erosion process that depends nonlinearly on slope. His elegant solutions are difficult for the non-mathematician to emulate but contain many features of the solutions derived, independently, in this paper. In particular, Luke identifies migrating knickpoints, physically unrealized portions of the solution, and information loss around migrating knickpoints.

[11] Weissel and Seidl [1998] built on the work of Luke [1972], using the method of characteristics to investigate the transient evolution of river profiles under a set of limited conditions. In particular, they solved the stream power equation for all  $n > 0$  provided that  $q(x, t) \sim x$ . Like Luke [1972], they showed that the solutions can become multi-valued, such that some portions of the solution are physically unrealized. They also showed that migrating knickpoints develop asymmetrically under these conditions, with concave-up knickpoints developing when  $n < 1$  and concave-down knickpoints developing when  $n > 1$ .

[12] More recent theoretical work was carried out by Whipple and Tucker [1999] who examined the case of steady state uplift for spatially varying uplift rates, as well as relaxation of perturbations from the steady state. They showed that the stream profile in steady state is given by (in our notation)

$$h_{ss} = \int_0^x \left[ \frac{u(x')}{q(x')} \right]^{1/n} dx' \quad (3)$$

[13] They also examined the pattern of upstream migration of river geometries when downstream portions of the river are instantaneously displaced from the steady state. They showed how the non-steady state component of the stream profile has a distinctive shape and migrates upstream with a characteristic time that depends on the erosional parameters of the river. In particular, they showed that whenever

uplift rates are constant in time, the rate of vertical migration of each elevation “patch” is also constant.

[14] Pritchard *et al.* [2009] analyzed the transient behavior of the stream power equation with the goal of using river profiles to constrain rock uplift histories. Like Weissel and Seidl [1998], they showed that solutions can become multi-valued, and they recognized that this implies a loss of information about the time history of the downstream boundary. Their approach, which focuses on the upstream propagation of a rescaled measure of channel slope, is similar in some respects to the approach we describe in section 5.

[15] Besides these works, there has been relatively little analytical work on erosion in response to the stream power equation, probably because its nonlinear form makes analysis difficult.

## 4. Non-Dimensionalization of the Stream Power Equation

### 4.1. General Equations

[16] In order to derive time-dependent solutions to the stream power equation, we make equation (1) dimensionless in a particular way that removes the effect of drainage area and other factors on the steepness of a river channel. This simplifies the equation and clarifies the principles involved. We define the following dimensionless variables (see also Table 1):

$$\tau = \frac{r_o A_o^m}{h_o} \int_0^t p(t')^m dt' \quad (4)$$

$$\chi = \frac{r_o^{1/n} A_o^{m/n}}{h_o} \int_0^x \frac{dx'}{r(x')^{1/n} A(x')^{m/n}} \quad (5)$$

$$v(\chi, \tau) = \frac{u(x, t)}{r_o A_o^m p(t)^m} \quad (6)$$

$$\lambda(\chi, \tau) = \frac{h(x, t)}{h_o} \quad (7)$$

where  $\tau$ ,  $\chi$ ,  $v$ , and  $\lambda$  are dimensionless time, distance, uplift rate, and river elevation, respectively.  $A_o$ ,  $r_o$ , and  $p_o$  are chosen reference values of drainage area, erodibility, and precipitation, and  $h_o$  is a chosen length scale. (If desired, we can choose  $h_o$  to be one in units of elevation, which has the advantage of “preserving” the value of elevation in the transformation to dimensionless units.) In these dimensionless units, the evolution equation for the river profile becomes

$$\frac{\partial \lambda}{\partial \tau} = v(\chi, \tau) - \left( \frac{\partial \lambda}{\partial \chi} \right)^n \quad (8)$$

[17] For the special case of  $n=1$ , there is a general solution to this equation (section A). For other values of  $n$ , this equation is nonlinear and more difficult to solve. In this paper and its appendices, we give solutions to two particular cases, one in which  $v$  is spatially invariant (has no  $\chi$  dependence) and another in which  $v$  is temporally invariant (has no  $\tau$  dependence). Before proceeding to these solutions, we first demonstrate some of the advantages of displaying longitudinal river profiles in terms of these dimensionless variables. A more thorough analysis and discussion of the methods and benefits of non-dimensionalization, with examples, is given in Perron and Royden [2013].

#### 4.2. Linearity of Steady State River Profiles

[18] Non-dimensionalization removes the effect of the downstream increase in drainage area. Thus, under uniform uplift, the concave-up longitudinal profile of a steady state river in dimensional coordinates becomes a straight profile in dimensionless coordinates. This is illustrated by rewriting equation (8) for the case in which  $v$  is uniform in space and time and the river is in steady state, so that the time derivative of  $\lambda$  is zero:

$$\frac{d\lambda}{d\chi} = v^{1/n} \quad (9)$$

[19] In this case, the slope of the dimensionless river profile depends only on the dimensionless uplift rate  $v$  and the slope exponent  $n$ , and the steady state profile is linear when  $v$  is spatially invariant.

[20] To illustrate this effect of the non-dimensionalization, we analyze two rivers in close proximity that are believed to be in steady state with respect to different, known uplift rates. We selected Juan and Shipman Creeks in the King Range of northern California, where sharp spatial gradients in uplift rates associated with the passage of the Mendocino Triple Junction have been inferred from uplifted marine terraces [Merritts and Bull, 1989; Merritts and Vincent, 1989]. Main stem longitudinal profiles and drainage areas were extracted from the  $\frac{1}{3}$  arc second (approximately 10 m) resolution NED using the procedure described in section 4.2. Bedrock sections of the profiles were identified using the drainage area limits determined by Snyder *et al.* [2000].

[21] If precipitation, erodibility, and uplift rate are uniform and constant for the two individual rivers, but potentially differ between the rivers, then we can non-dimensionalize using  $r(x) = r_0$  for both. Figure 1 shows the two river profiles in dimensional and the resulting dimensionless units. In dimensional coordinates (Figure 1a), the river profiles are concave up. This curvature makes it difficult to distinguish potential knickpoints from reaches with smoothly varying transient geometries. When the profiles are plotted in dimensionless coordinates (Figure 1b), they take on a nearly linear form, suggesting that they are nearly at steady state, with slight deviations from linearity corresponding to minor spatial or temporal inhomogeneities in incision.

#### 5. Slope Patches

[22] In this and the following sections, we explore the behavior of river profiles governed by the stream power law using the concept of “slope patches.” A river longitudinal profile evolving according to the stream power law consists of a series of contiguous segments, or “patches,” of slope. In dimensionless variables, these migrate upstream at a rate that depends only on the slope of the individual patch and on the slope exponent,  $n$  (Figure 2). The slope of a patch is equal to the derivative of elevation with respect to horizontal position. In dimensionless coordinates, this slope is

$$\sigma(\chi, \tau) = \frac{\partial \lambda}{\partial \chi} \quad (10)$$

[23] A slope patch is not a physical object associated with a particular parcel of bedrock but rather a mathematical entity that propagates up a river profile and carries

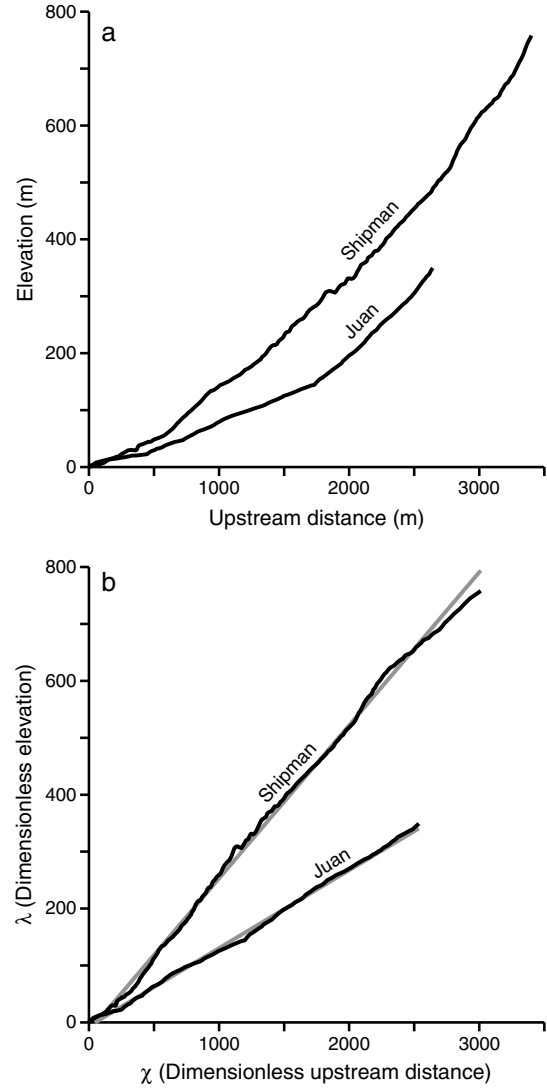


**Figure 1.** (a) Longitudinal profiles of Juan and Shipman Creeks in the northern California King Range. Profiles were extracted from the  $\frac{1}{3}$  arc second U.S. National Elevation Dataset, with bedrock sections identified based on the drainage area bounds of Snyder *et al.* [2000]. (b) Dimensionless longitudinal profiles for  $A_0 = 10^6 \text{ m}^2$ ,  $h_0 = 1 \text{ m}$ ,  $r_0 = r = 1 \text{ m}^{1-3m} \text{ yr}^{m-1}$ ,  $n = 1$ , and  $m/n = 0.4$ . Gray lines are least-squares linear fits to the dimensionless profiles.

information about the state of the river downstream. Information can travel only as fast as the slope patch that carries it.

[24] The equations that govern the behavior of slope patches permit analytical solutions to the stream power equation for the case of spatially invariant (but time-varying) uplift rates. (Time-invariant, but spatially variable, uplift is amenable to quasi-analytical solutions that are stepwise in time.) Slope patch analysis provides insight into the behavior of migrating knickpoints, explaining why some migrating knickpoints remain sharply defined while others spread with time. Slope patch analysis also sheds light on how information about events occurring at base level propagates upstream and how information about past states of the river profile can be progressively lost at migrating knickpoints. In the following sections, we explore slope patch behavior and knickpoint

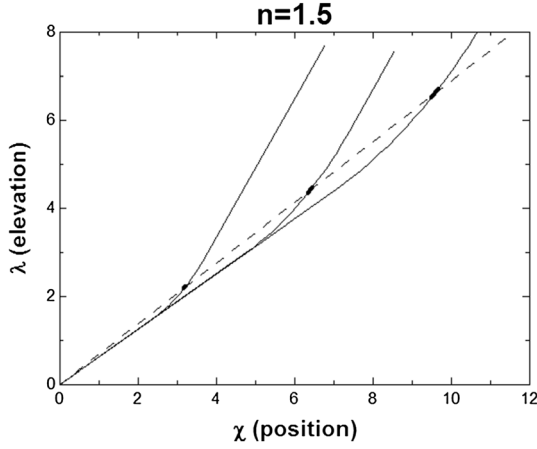


**Figure 2.** Example of a slope patch (heavy line segment) migrating upstream, lower left to upper right, at three instants separated by dimensionless time intervals  $\Delta\tau=4$  during the evolution of a river profile. Solid lines show successive river profiles, and the dashed line shows the path of the slope patch through time. If there is no lateral variation in uplift rate, the slope of the patch will remain constant through time, as in this example, and the horizontal and vertical rates of slope patch migration will also remain constant. See Table 3 for values used.

migration in dimensionless coordinates, and derive analytical solutions for cases of particular interest.

## 6. River Profiles for Spatially Invariant Uplift Rates

[25] The kinematics of a single slope patch for spatially invariant uplift rates are relatively simple when expressed in dimensionless variables, but the evolution of a longitudinal river profile is more complex because it consists of a series of connected slope patches that may migrate upstream at different rates. Because the dimensionless form of the stream power equation renders the conceptual and quantitative aspects of slope patches much simpler than the dimensional form, we use dimensionless variables throughout sections 6. Unless stated otherwise, river profiles and all variables are dimensionless.

[26] Equations for the elevation and horizontal position of slope patches in a system where uplift rate is spatially invariant are derived in section B. For simplicity, we assume no initial topography (a horizontal profile with zero elevation) in the cases presented in the main text. The solution with initial topography is given in section B. The relevant equations are

$$\lambda = (n-1)(\tau - \tau_i)v(\tau_i) + \int_{\tau_i}^{\tau} v(\tau')d\tau' \quad (11)$$

$$\chi = n(\tau - \tau_i)v(\tau_i)^{(n-1)/n} \quad (12)$$

where we have introduced a new variable  $\tau_i$  such that elevation and horizontal position are functions of  $\tau$  and of  $\tau_i$ .  $\tau_i$  is the time at which the  $i$ th slope patch is created at base level. When  $\tau$  equals  $\tau_i$ , then  $\chi$  and  $\lambda$  are zero.

[27] The river gradient, and equivalently the gradient of the corresponding slope patch, is found by taking the derivative of equation (11) with respect to  $\chi$  while holding  $\tau$  fixed.

[28]

$$\sigma(\chi, \tau) = \frac{\partial \lambda}{\partial \chi} = v(\tau_i)^{1/n} \quad (13)$$

$v(\tau_i)$  is the bedrock uplift rate at time  $\tau_i$ , when the  $i$ th slope patch was created at base level. The horizontal rate of motion of the  $i$ th slope patch as it moves along the river profile is found by taking the time derivative of equation (12) while holding  $\tau_i$  fixed:

$$\frac{\partial \chi}{\partial \tau} = n v(\tau_i)^{(n-1)/n} = n \sigma^{n-1} \quad (14)$$

[29] The vertical rate of motion of the  $i$ th slope patch can be obtained by taking the derivative of equation (11) with respect to  $\tau$  while holding  $\tau_i$  fixed.

$$\frac{\partial \lambda}{\partial \tau} = (n-1)v(\tau_i) + v(\tau) = (n-1)\sigma^n + v(\tau) \quad (15)$$

[30] Note that this expression for the rate of vertical motion is not the rate of change of elevation at a fixed position. It is the rate of change of elevation of a slope patch as it migrates up the river.

[31] The preceding equations show that for spatially invariant uplift rates, the slope of a patch does not change during upstream migration. This is illustrated by the slope patch in Figure 2, shown by the dark line segments superimposed on a succession of river profiles. The slope of the patch is constant in time. The rate of migration of the slope patch is constant in  $\chi$  and  $\lambda$ , so that the trajectory of the slope patch is a straight line. The slope of this trajectory is not the same as the slope of the patch nor is it the same as the slope of the river at steady state. The patch trajectory will, however, coincide with both when the river profile is in steady state.

[32] The rate of horizontal migration of a slope patch in dimensionless units (but not in dimensional units) depends only on  $n$  and the slope of the patch, whereas the rate of vertical migration of each slope patch in both dimensional and dimensionless units depends on  $n$ , on its slope, and on the rate of uplift. Whenever uplift rates relative to base level are constant in time and spatially invariant, the dimensionless rate of horizontal migration of each slope patch is constant (equation (14)), while the rate of vertical migration of each slope patch is constant in non-dimensional and dimensional units (equation (15)). The latter insight was used by *Whipple and Tucker* [1999] and *Whipple* [2001] to estimate landscape response time to a single step change in uplift or climate.

[33] In the special case where  $n=1$ , all slope patches migrate horizontally at a rate equal to one in dimensionless units (see also general solution for  $n=1$  in section A). When  $n$  is not equal to 1, slope patches with different slopes migrate at different rates. Steeper patches migrate faster for  $n > 1$ , and flatter patches migrate faster for  $n < 1$  [see also *Weissel and Seidl*, 1998 and *Pritchard et al.*, 2009].

[34] In dimensional variables, the slope of each patch does not remain constant but varies with erodibility ( $r$ ), drainage area ( $A$ ), precipitation ( $p$ ), and other factors (equations (1) and (2)). The rate of horizontal migration depends on the slope of the patch and also on  $r$ ,  $A$ ,  $p$ , and other factors. The relative complexity of the dimensional expressions

illustrates the power of the dimensionless form in providing a conceptual understanding of evolving river profiles.

### 6.1. River Profile Response to Instantaneous Changes in Uplift Rate

[35] Equations (11) and (12) (or equivalently equations (14) and (15)) can be used to construct dimensionless river profiles. The procedure begins by defining a series of slope patches generated at base level at times  $\tau_i$ . The horizontal and vertical positions of each slope patch can be computed at any chosen time  $\tau$ , and the collective position of all slope patches, plus interpolation between patches, yields the dimensionless river profile. This process is not completely straightforward and is described in more detail in section C.

#### 6.1.1. Instantaneous Change in Uplift Rate, $n > 1$

[36] For  $n > 1$ , consider a river profile in steady state experiencing uplift relative to base level at a rate  $v_1$ . The river profile will have a uniform slope in dimensionless coordinates consisting of slope patches with a slope of  $v_1^{1/n}$  (equation (13)). Subsequently, at time  $\tau = \tau_2$ , the uplift rate decreases abruptly to a new, slower rate  $v_2$  and is then held constant. New slope patches will be generated at base level. These younger slope patches will be less steep than the older patches and will have a slope of  $v_2^{1/n}$ .

[37] The slope patches generated before and after  $\tau_2$  travel horizontally upstream at different rates. The steeper upstream patches generated before  $\tau_2$  travel faster, at a rate  $nv_1^{(n-1)/n}$ , whereas the flatter downstream patches generated after  $\tau_2$  travel slower, at a rate  $nv_2^{(n-1)/n}$ . Therefore, a gap opens up between the last slope patch generated before  $\tau_2$  and the first slope patch generated after  $\tau_2$  (Figure 3a). However, the river profile must be continuous. The river profile in this gap can be computed by requiring the uplift rate relative to base level to also be a continuous function of time.

[38] Consider an uplift rate that decreases smoothly and monotonically from  $v_1$  to  $v_2$  from time  $\tau = \tau_2$  to  $\tau = \tau_2 + \varepsilon$ . In this interval of time, multiple slope patches with slopes between  $v_1^{1/n}$  and  $v_2^{1/n}$  are generated at base level. We can take the limit as  $\varepsilon$  goes to 0 and note that  $\varepsilon$  can be made arbitrarily small. We obtain a three-component solution for the evolving river profile using equations (11) and (12), to find (Figure 3):

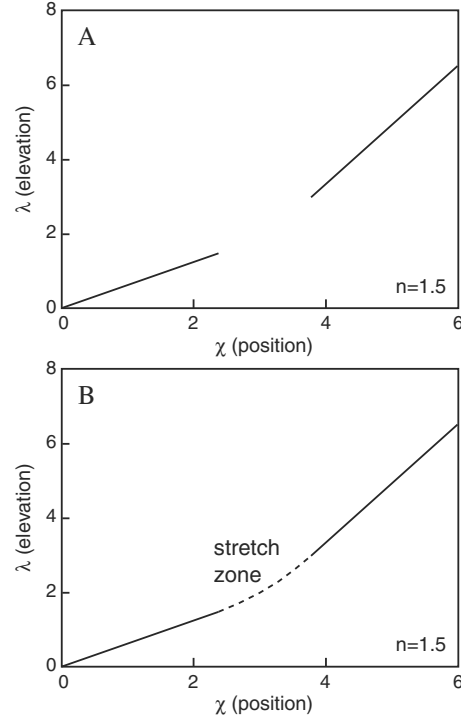


**Figure 3.** (a) A fast uplift rate ( $v=2.0$ ) forms a relatively steep river gradient. This is followed by a slower uplift rate ( $v=0.5$ ) that forms a relatively gentle river gradient (equations (16a) and (16c)). These linear segments (shown by solid lines) separate progressively because the steeper slope patches travel upstream faster than the less steep slope patches. (b) The ends of the linear segments are connected by a series of slope patches created during the instantaneous change in uplift rate from fast to slow (dashed line). These form a “stretch zone” with a characteristic curved shape of the form given in equation (16b).

[39] The first component (equation (16a)) “grows” out of the time interval before  $\tau_2$ , when uplift is maintained at  $v_1$  (Figure 3a). The third component (equation (16c)) grows out of the time interval after  $\tau_2$ , when uplift is maintained at  $v_2$  (Figure 3a). The second component (equation (16b)) grows

$$\lambda = \begin{cases} \chi v_1^{1/n} + (\tau - \tau_2)(v_2 - v_1) & \tau_i \leq \tau_2; \chi \geq \chi_1 \\ \frac{n-1}{n} \left( \frac{\chi^n}{n(\tau - \tau_2)} \right)^{\frac{1}{n-1}} + (\tau - \tau_2)v_2 & \tau_i = \tau_2; \chi \text{ between } \chi_1 \text{ and } \chi_2 \\ \chi v_2^{1/n} & \tau_i \geq \tau_2; \chi \leq \chi_2 \end{cases} \quad (16a)$$

$$\tau_i = \tau_2; \chi \text{ between } \chi_1 \text{ and } \chi_2 \quad (16b)$$

$$\tau_i \geq \tau_2; \chi \leq \chi_2 \quad (16c)$$

with

$$\chi_1 = n(\tau - \tau_2)v_1^{(n-1)/n} \quad (16d)$$

$$\chi_2 = n(\tau - \tau_2)v_2^{(n-1)/n} \quad (16e)$$

out of the infinitesimally short time interval around time  $\tau_2$  when the uplift rate changes from  $v_1$  to  $v_2$ . This curve consists of slope patches of varying slope that were created at time  $\tau_2$  but that travel upstream at different rates because they have different slopes (equation (16b) and Figure 3b). The horizon-

tal rate of upstream migration of these slope patches is proportional to the slope of the patch raised to the power  $(n - 1)$ . Thus, the second component of the stream profile consists of slope patches all created at a single moment, or vanishingly short moment, in time. We call this part of the profile a “stretch zone” because it begins from a single point and expands as the slope patches created at that point migrate upstream and spread apart (Figure 3).

[40] Now consider the converse case, also for  $n > 1$ , for a river profile in steady state during uplift relative to base level at a rate  $v_1$ . As before, the river profile will consist of patches with a uniform slope given by substituting  $v_1$  into equation (13). Subsequently, at time  $\tau = \tau_2$ , the uplift rate increases abruptly to a new, faster rate  $v_2$  and is then held constant. New slope patches will be generated at base level, and the younger slope patches will be steeper than the older slope patches (Figure 4a).

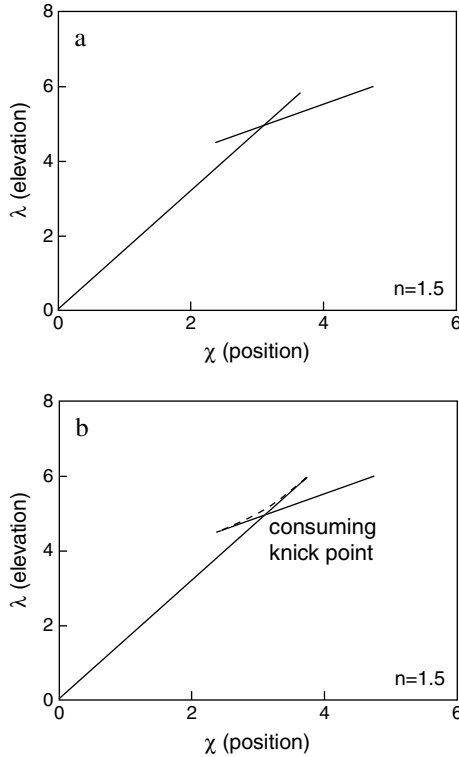


**Figure 4.** (a) A slow uplift rate ( $v=0.5$ ) forms a relatively gentle river gradient. This is followed by a faster uplift rate ( $v=2.0$ ) that forms a relatively steep river gradient (equations (16a) and (16c)). These linear segments (shown by dark lines) overlap progressively because the steeper slope patches travel upstream faster than the less steep slope patches. (b) The overlapping ends of each linear segment are connected by a series of slope patches created during the instantaneous change in uplift rate from fast to slow (dashed curved line). These form a characteristic curve of the form given in equation (16b). However, neither the overlapping portions of the linear profile segments nor the curved section consisting of slope patches created during the change in uplift rate are physically realized. The physically realized portion of the profile (heavy lines) consists of the two non-overlapping segments and a sharp knickpoint that migrates upstream.

[41] Once again, the slope patches generated before and after  $\tau_2$  travel upstream at different rates (equation (13)). In this case, however, the flatter, older upstream patches travel more slowly than the steeper, younger downstream patches. Therefore, an overlap quickly develops between the last slope patch generated before  $\tau_2$ , at uplift rate  $v_1$ , and the first slope patch generated after  $\tau_2$ , at uplift rate  $v_2$  (Figure 4a). The amount of overlap between the flatter, older section of the profile and the steeper, younger section of the profile increases over time.

[42] The structure of the slope patch solution for patches created around time  $\tau_2$  can be calculated by requiring that uplift rate increases smoothly and monotonically from  $v_1$  to  $v_2$  between time  $\tau = \tau_2$  and  $\tau = \tau_2 + \epsilon$ . In this interval of time, multiple slope patches with slopes between  $v_1^{1/n}$  and  $v_2^{1/n}$  are generated at base level, yielding a three-component solution for the evolving river profile that is once again given by equations (16a)–(16c). The first component “grows” out of the time interval before  $\tau_2$ , when uplift is maintained at  $v_1$ . The third component grows out of the time interval after  $\tau_2$ , when uplift is maintained at  $v_2$ . The second component—the stretch zone—grows out of the infinitesimally short time interval around time  $\tau_2$  when the uplift rate changes from  $v_1$  to  $v_2$ .

[43] Plotting this solution (Figure 4b) shows that  $\lambda$  is not a single-valued function of  $\chi$  but instead has multiple values in the region near the change in slope of the river profile [see also Luke, 1972 and Weissel and Seidl, 1998]. The interpretation of this is that not all parts of the solution are physically realized. All of the slope patches created are present in the mathematical solution (light dashed lines) but not in the physically realized river profile. In fact, none of the slope patches in the second component of the solution—the stretch zone—form part of the physically realized profile. Likewise, portions of the first and third components of the solution are not physically realized. The physically realized portions of the solution form an abrupt, concave-down knickpoint and adjacent line segments. In essence, slope patches have been lost from the river profile where the steeper, faster-moving slope patches have over-ridden the flatter, slower moving slope patches. We call this migrating knickpoint a “consuming knickpoint” because it consumes adjacent slope patches that disappear permanently from the physically realized solution.

[44] We can calculate the distance that this consuming knickpoint has traveled upstream, as a function of time, by calculating the intersection of the first and third components of equations (16a) and (16c):

$$\chi_{\text{knick}} = (\tau - \tau_2) \left[ \frac{v_2 - v_1}{v_2^{1/n} - v_1^{1/n}} \right] \quad (17)$$

[45] We can calculate the rate of horizontal knickpoint migration by dividing equation (17) by  $(\tau - \tau_1)$ .

$$\frac{\partial \chi_{\text{knick}}}{\partial \tau} = \left[ \frac{v_2 - v_1}{v_2^{1/n} - v_1^{1/n}} \right] \quad (18)$$

[46] The example of an abrupt change in uplift rates highlights a general property of evolving profiles: for  $n > 1$ , concave-up migrating knickpoints cannot be maintained and are replaced with a progressively more gradual transition between steeper and gentler slopes, whereas concave-down migrating knickpoints are maintained and can also form



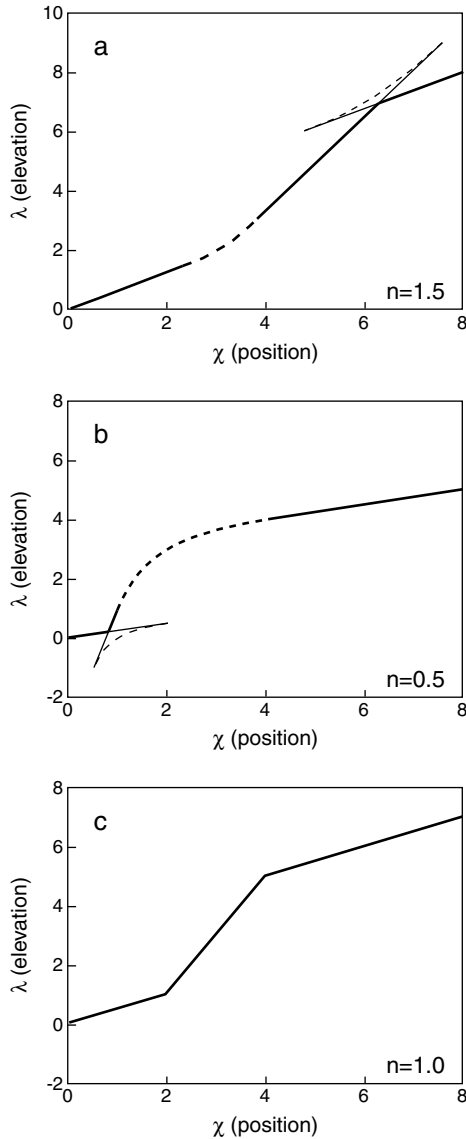


**Figure 5.** Characteristic river profiles formed by two instantaneous changes in uplift rate, first from  $v=0.5$  to  $v=2.0$ , followed by a change from  $v=2.0$  to  $v=0.5$ , for (a)  $n=1.5$ , (b)  $n=0.5$ , and (c)  $n=1.0$ . The straight, solid line segments consist of slope patches formed at base level during the periods of constant uplift rate. The curved, dashed sections formed during the moment of instantaneous change in uplift rate; for  $n=1$ , these curved sections are collapsed to a single point. Heavy solid and dashed lines are physically realized portions of the river profile; light solid and dashed lines are not physically realized but are still part of the slope patch solution.

during progressive evolution of the river profile. At concave-down knickpoints, slope patches are progressively lost, and therefore, information about older river profiles is also lost. Below, we show that this mathematical behavior of slope patches, with expansion of concave-up river sections and consumption of concave-down river sections, leads to a characteristic shape for these rivers that is fundamentally different from the case where  $n < 1$  or  $n = 1$ .

[47] We can use equation (16) twice to generate both a stretch zone and a consuming knickpoint on the same profile. Figure 5a shows the profile generated by a slow uplift rate

followed by a fast uplift rate followed by a slow uplift rate. This results in a consuming knickpoint (concave down) upstream and a stretch zone (concave up) downstream.

### 6.1.2. Instantaneous Change in Uplift Rate, $n < 1$

[48] When  $n < 1$ , the shapes of transient river profiles are different from the  $n > 1$  case, but many of the concepts used to understand the evolution of the profiles are similar. The difference in profile shapes has been noted previously by *Weissel and Seidl* [1998] and *Tucker and Whipple* [2002], based on both analytical and numerical modeling approaches. Here we show that the fundamentally different shapes of the transient solutions for differing  $n$  can be attributed to the way in which slope patch solutions govern the development of stretch zones and migrating knickpoints.

[49] The solutions given in equation (16) also apply to the case of  $n < 1$ . Figure 5b illustrates these principles for  $n < 1$ . This figure shows the profile generated by a slow uplift rate, followed by a fast uplift rate, and followed by a slow uplift rate, as in Figure 5a. This results in a stretch zone (concave down) upstream and consuming knickpoint (concave up) downstream.

[50] This profile geometry can be understood by considering a river profile in steady state that is experiencing uplift relative to base level at a rate  $v_1$ . The river profile will again consist of patches with a uniform slope given by equation (16a). Subsequently, at time  $\tau = \tau_2$ , the uplift rate increases abruptly to a new, faster rate  $v_2$  and is then held constant. New slope patches will be generated at base level. These younger slope patches will be steeper than the older patches, but because  $n < 1$ , the steeper patches will travel upstream more slowly than the flatter, older slope patches. As before, a gap opens up between the last slope patch generated before  $\tau_2$  and the first slope patch generated after  $\tau_2$ . The solution to the evolving river profile is given by equation (16) and has three components, with the second component being a stretch zone consisting of slope patches all created in a single moment at time  $\tau = \tau_2$ .

[51] Conversely, consider a steady state river profile that experiences an abrupt decrease in uplift rate from  $v_1$  to  $v_2$  at time  $\tau = \tau_2$ . New slope patches will be generated at base level, and younger slope patches will be flatter than the older patches. The steeper upstream patches travel more slowly than the flatter downstream patches, and an overlap develops between the last slope patch generated before  $\tau_2$ , at uplift rate  $v_1$ , and the first slope patch generated after  $\tau_2$ , at uplift rate  $v_2$ . The complex structure of the solution for slope patches generated around time  $\tau_2$  is similar to that computed for the increased uplift rate with  $n > 1$  and is also given by equation (16b). However, in this case, the multi-valued solution for elevation occurs at a concave-up knickpoint, which forms a consuming knick point. All of the second component of the solution of equation (16)—the stretch zone—and parts of the first and third components are within this region of multiple values and are not part of the physically realized solution. The flatter, faster-moving slope patches have over-ridden the steeper, slower moving slope patches, and the intervening slope patches have been “lost.”

[52] Thus, for  $n < 1$ , concave-down migrating knickpoints cannot be maintained, while concave-up migrating knickpoints are maintained and can also form during progressive evolution of the river profile. At concave-up knickpoints, slope patches are progressively lost, and therefore, information about older river profiles is also lost.

### 6.1.3. Instantaneous Change in Uplift Rate, $n = 1$

[53] The same analysis can be performed for the special case of  $n = 1$ . In this case, all slope patches migrate horizontally upstream at a rate equal to one, independent of slope. The solution in equation (16b) collapses to a point, and the river segments corresponding to equations (16a) and (16c) neither have a gap nor overlap between solutions. Slope patches are neither lost nor generated at migrating knickpoints, and all migrating knickpoints are preserved (Figure 5c).

## 6.2. River Profile Response to Oscillating Uplift Rates

[54] Equation (16) can be used multiple times with uplift alternating between  $v_1$  and  $v_2$  at intervals of  $\frac{T}{2}$  to produce an oscillating uplift rate with period  $T$  and an average uplift rate of  $(v_1 + v_2)/2$ . This allows one to see if departures in uplift rate from a mean rate disappear upstream and, if so, how far upstream the variations in uplift rate persist. The results therefore give timescales and length scales over which variations in uplift rate will persist upstream. These results, which extend the principles illustrated in Figure 5, are plotted in Figure 6.

### 6.2.1. Profiles for Oscillating Uplift Rates, $n = 1$

[55] In the special case where  $n = 1$ , the slope patches created during fast and slow uplift migrate upstream at the same rate. All slope patches are preserved in the physically realized portion of the solution, and the river elevation profile is simply a set of alternating linear segments that migrate upstream without modification (Figure 6a). The complete uplift history at the downstream end of the profile can be reconstructed from the slopes of these river segments, and no information about uplift history is lost.

### 6.2.2. Profiles for Oscillating Uplift Rates, $n > 1$

[56] When  $n > 1$ , steeper slope patches migrate faster than the less steep patches. The steep slope patches generated at the downstream boundary migrate upstream with increasing overlap with the flatter, more slowly migrating segments. Eventually, the overlap between the linear river segments (equations (16a) and (16c)) is so great that the linear segments disappear and are not part of the physically realized solution. Instead, only stretch zones, generated at the transition from fast to slow uplift rate, exist in the physically realized solution (Figure 6b and equation (16b)). The average gradient of the river eventually becomes the gradient that would have been generated by the average uplift applied continuously at the downstream boundary.

[57] The point at which the linear river segments disappear depends on  $n$  and on the contrast between the fast and slow rates of uplift. We can approximate the distance up the river at which the linear river segments disappear as the position where the back of the faster-moving linear segment overrides the front of the slower moving linear segment. In this case, no part of the slower moving linear segment is part of the physically realized solution.

[58] Suppose the slope patch at the upstream end of the slower moving segment is generated at time  $\tau_1$  at an uplift rate  $v_1$ . The distance traveled horizontally by this slope patch after a time  $\tau$  is

$$\chi = n(\tau - \tau_1)v_1^{(n-1)/n} \quad (19)$$

[59] The slope patch at the downstream end of the faster-moving segment is subsequently generated at time  $\tau_1 + T$  at

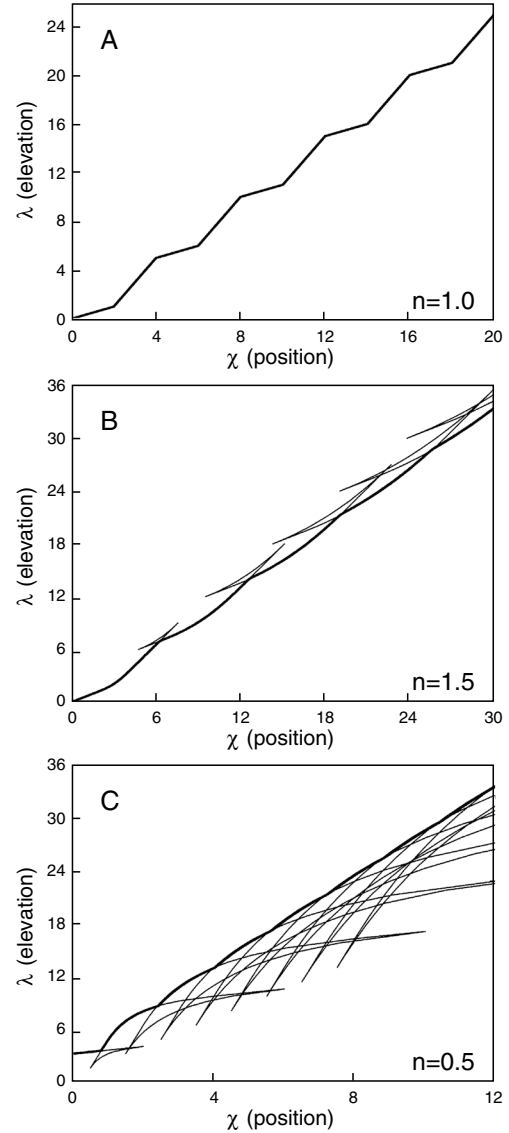


**Figure 6.** River profiles formed by oscillating instantaneous changes in uplift rate, between  $v = 0.5$  and  $v = 2.0$ , with a dimensionless period  $T = 4$ . The straight line segments consist of slope patches formed at base level during periods of constant uplift rate. The curved sections of the river profile represent slope patches formed during each instantaneous change in uplift rate; for  $n = 1$ , these curved sections are collapsed to a single point. (a) For  $n = 1$ , the entire profile is physically realized. (b, c) The physically realized portion of the river profile is the envelope curve (dark line) corresponding to the smallest value of  $\lambda$  for  $n > 1$  and the largest value of  $\lambda$  for  $n < 1$ . For  $n < 1$  and  $n > 1$ , discrete slope sections created at base level, with alternating slopes, disappear upstream and are replaced by a nearly linear river profile with a slope corresponding to the average uplift rate.

an uplift rate  $v_2$ . The distance traveled horizontally by this slope patch after a time  $\tau$  is

$$\chi = n(\tau - \tau_1 - T)v_2^{(n-1)/n} \quad (20)$$

[60] Setting the two values of  $\tau$  equal in equations (19) and (20) and solving for  $\chi$  yield

$$\chi = \frac{nT}{v_1^{(1-n)/n} - v_2^{(1-n)/n}} \quad (21)$$

[61] For the values of  $T$  (4),  $v_1$  (0.5), and  $v_2$  (2) used in Figure 6b, this yields a value of  $\chi$  equal to  $\sim 12$  for  $n=1.5$ . Inspection of Figure 6b shows that this is essentially correct.

### 6.2.3. Profiles for Oscillating Uplift Rates, $n < 1$

[62] The response of longitudinal river profiles with  $n < 1$  to oscillating uplift rate is similar to that of profiles with  $n > 1$ . The primary difference is that flatter slope patches migrate faster than the steep slope patches. Thus, slope patches generated at the transition from fast to slow uplift rates take over the entire profile. The horizontal distance over which this occurs is also given by equation (19) in the case where  $n < 1$ . For the values of  $T$  (4),  $v_1$  (2), and  $v_2$  (0.5) used in Figure 6c, this yields a value of  $\chi$  equal to  $\sim 4$  for  $n=0.5$ . Inspection of Figure 6c shows that this is again essentially correct.

[63] It is apparent that upstream portions of longitudinal river elevation profiles do not contain complete information about uplift rates at the downstream boundary unless  $n = 1$ . For oscillating rates of uplift, one can in practice determine the average uplift rate (from the slope) and possibly the period of the oscillation (from the length of the concave river segments), but little else. At distant upstream locations, oscillations in base level would be practically impossible to determine from river elevation data. This occurs because information is lost at migrating knickpoints and slope patches generated at the transition from slow to fast uplift rates take over the entire profile.

## 7. Uplift Rates that Vary in Space

[64] Similar to the case in which uplift rates are spatially invariant, the evolution of rivers in regions of spatially and temporally varying uplift rates can also be understood as the upstream migration of a series of slope patches. However, when uplift rates vary spatially, the gradient of each slope patch will not remain constant during upstream migration but will change in a manner that depends on the local uplift rate and on the uplift rate where the slope patch was formed. Section D contains a mathematical treatment of the case in which uplift rates vary spatially but not temporally and in which the river profile may have nonzero initial elevations.

[65] This method for treating spatially variable, but temporally invariant, uplift rates applies to continuously varying uplift rates as a function of position. However, in the discussion below, we confine our remarks to spatially varying uplift consisting of a series of blocks uplifted at different rates.

### 7.1. Stationary Versus Migrating Knickpoints

[66] Our results show that when uplift rates are spatially variable, two fundamentally different types of knickpoints may develop. Wherever there are abrupt spatial changes in uplift rate, stationary knickpoints develop that may be concave up or down for any value of  $n$ . These stationary knickpoints are always pinned to the position where basement uplift rates change, such as above an active fault zone; they do not migrate upstream.

[67] In addition, migrating knickpoints or stretch zones form where there is variation in initial (dimensionless) slope between upstream and downstream river segments. These

migrating knickpoints are identical in behavior to the knickpoints and stretch zones produced at base level for spatially invariant uplift. The migrating knickpoints are always concave down for  $n > 1$  and concave up for  $n < 1$  and are always consuming knickpoints (except when  $n = 1$ ). Portions of the mathematical solution are not physically realized at these migrating knickpoints, and information about previous river profiles is progressively lost. Like the case of spatially invariant uplift, migrating knickpoints that are concave up cannot be maintained for  $n < 1$ , and migrating knickpoints that are concave down cannot be maintained for  $n > 1$ .

### 7.2. Profiles With Spatially Variable (Time-Invariant) Uplift Rates

[68] The difference between stationary and migrating knickpoints is illustrated by the river profiles computed in Figure 7. The initial topography consists of a moderately steep slope in

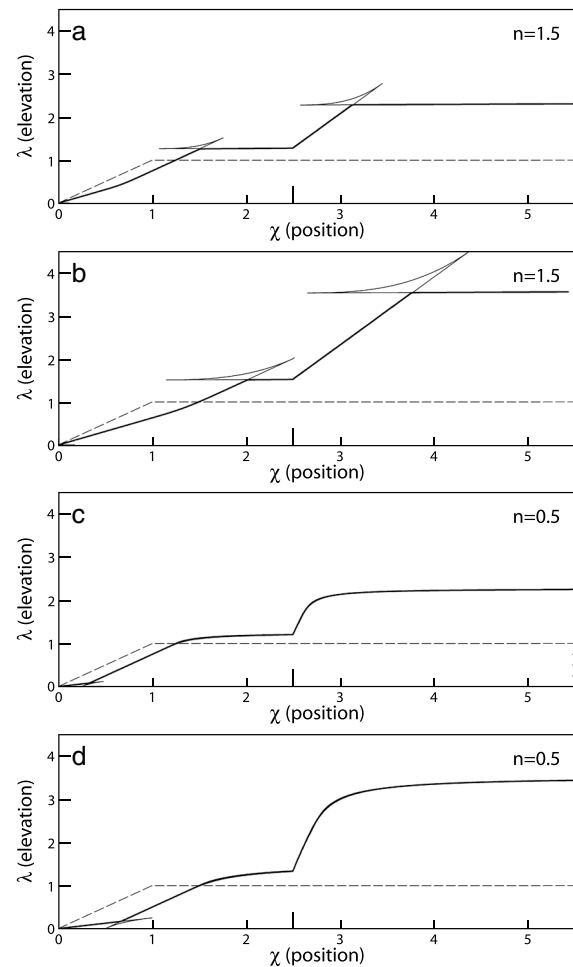


**Figure 7.** River profiles formed by spatially varying uplift at a constant rate with initial topography (dashed line). Uplift rates are  $v=0.5$  for  $\chi < 2.5$  and  $v=2.0$  for  $\chi > 2.5$ . Dark line is the river profile computed from forward-time, upwind (downstream) finite differencing overlaid on the slope patch solution. The two solutions overlap very closely except where the slope patch solution is not physically realized. Note the presence of a stationary knickpoint at location  $\chi=2.5$ , where there is a change in uplift rate. (a)  $n=1.5$ ,  $\tau=0.5$ ; (b)  $n=1.5$ ,  $\tau=1.0$ ; (c)  $n=0.5$ ,  $\tau=0.5$ ; (d)  $n=0.5$ ,  $\tau=1.0$ .

the downstream part of the river and a horizontal highland region in the upstream part of the river. Uplift occurs at a constant rate ( $v=0.5$ ) for  $\chi < 2.5$  and a faster constant rate ( $v=2.5$ ) for  $\chi > 2.5$ . (The two time slices shown in the profile evolution do not include the final steady state.)

[69] For the case where  $n = 1.5$ , a concave-down knickpoint is developed at the slope break initially at  $\chi = 1.0$  and migrates upstream. A concave-up stationary knickpoint is developed over the central highland region, corresponding to the zone where basement uplift rates increase upstream. This knickpoint will remain fixed and will eventually be present in the steady state solution to the river profile. A concave-down knickpoint is formed initially at the zone where basement uplift rates increase upstream, and this knickpoint migrates upstream.

[70] Unlike the solution in the vicinity of migrating knickpoints, the solution for the river profile is not multi-valued in the region of a stationary knickpoint and there is no physically unrealized portion of the solution. Hence, information about previous river profile states is not lost at stationary knickpoints but is carried upstream by slope patches as they cross these knickpoints.

[71] Stationary knickpoints may arise in dimensioned river profiles from a variety of causes, such as abrupt spatial changes in bedrock erodibility, precipitation rate, or uplift rate. Provided the stream power model applies, however, such knickpoints

can be removed with proper non-dimensionalization (equations (4)–(7)) and theoretically should not appear as knickpoints in the corresponding dimensionless profiles.

## 8. Comparison With Standard Numerical Methods

[72] The slope patch analysis developed in this paper is valuable because of the insight it provides into the development of river profiles and the ability to compute various quantities analytically. It is, however, more difficult to use than standard finite-difference techniques (section C). For example, one must always guarantee a sufficient density of slope patches migrating up a river, which can be difficult when slope patches on a horizontal surface move at either infinite ( $n < 1$ ) or zero ( $n > 1$ ) speed. Still, the ability to calculate an analytical solution for transient river profile evolution provides an important test of the accuracy of numerical solutions.

[73] Provided that  $n$  is not too close to 1, the results of slope patch analysis compare well to numerical solutions of the stream power equation that are based on standard finite-difference methods. Figures 6 and 7 give solutions for an evolving river profile derived from slope patch analysis (light lines) and solutions to the same problems computed from a finite-difference approximation of equation (8) for a dimensionless uplift rate of  $v = 4$ . The finite-difference scheme uses forward differencing in time and upwind (downstream)

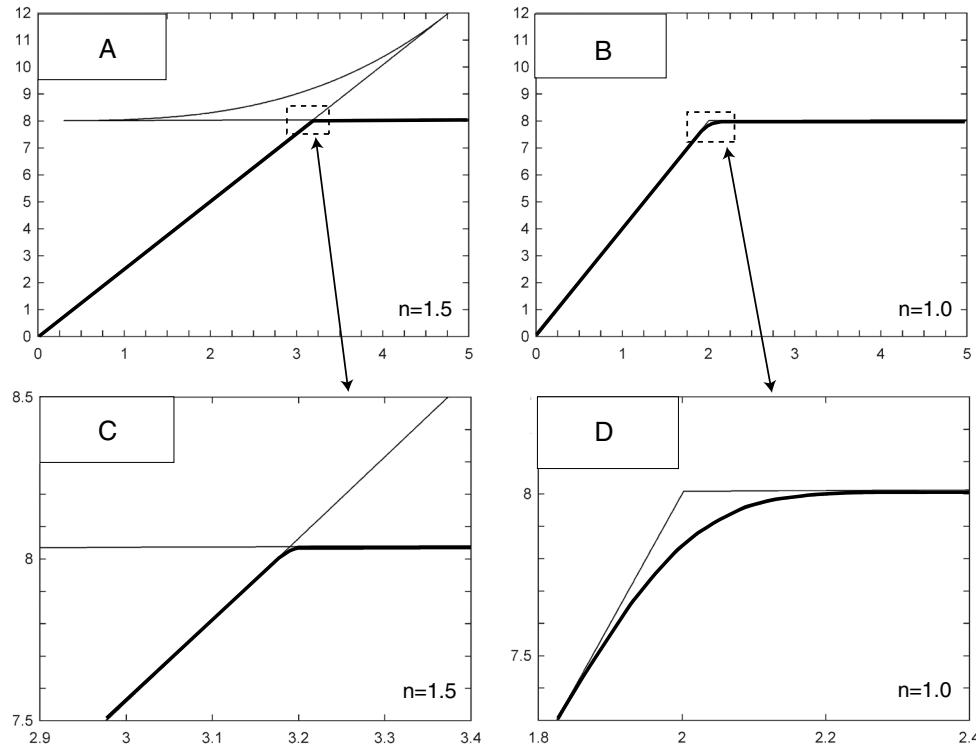


**Figure 8.** Detailed evolution of a migrating knickpoint showing differences between analytical slope patch solutions (light lines) and finite-difference solutions with forward-time, upwind differencing (heavy lines) at a dimensionless uplift rate of  $v = 4$ . A knickpoint is produced by uplift of an initially horizontal surface. (c) and (d) are details of (a) and (b), respectively, as indicated by dashed boxes. The finite-difference solution incorrectly produces significant diffusive rounding at the knickpoint for  $n = 1$  and slight diffusive rounding for  $n = 1.5$ . The slope patch solution correctly maintains a sharp knickpoint in both instances.

differencing with a grid point spacing of 0.005 to compute the slope (dark lines) for values of  $n = 1.5$  and  $n = 0.5$ . The agreement is excellent, with the finite-difference solution plotting immediately on top of the solution produced by slope patch analysis. The numerical solution contains none of the physically unrealized parts of the slope patch solution, which is expected, and it is straightforward to remove the physically unrealized portions of the slope patch solution.

[74] For  $n = 1.5$  and  $n = 0.5$ , the numerical solutions plot almost immediately on top of the slope patch solution even at migrating and stationary knickpoints where the slopes of the river profile are discontinuous. When  $n = 1$ , however, the migrating knickpoints are sharply defined for the slope patch solutions but somewhat rounded by the diffusive nature of the numerical solution (Figure 8). In this case, the two solutions do not agree precisely, and it is the slope patch solution that is correct (see also analytical solution for  $n = 1$  in section A).

[75] The slope patch solution thus provides a way to evaluate the accuracy of transient numerical solutions before applying a numerical method to more complex scenarios of river profile evolution. If the accuracy is found to be insufficient, a different numerical method can be chosen. Alternatively, closer spacing of grid points or shorter time steps in the numerical method can provide increased accuracy in the numerical solution, while coarser grid spacing, longer time steps, and longer duration simulations will result in larger errors. Upwind differencing is widely used for transport or advection problems, of which the stream power equation is one example, but it is only first-order accurate in space, with consequences like those illustrated in Figure 8. One way to improve on simple upwind differencing that still takes advantage of the property that information propagates up river profiles is to use an interpolation-based advection scheme that offers better fidelity, such as a semi-Lagrangian method [Staniforth and Côté, 1991; Spiegelman and Katz, 2006]. Another strategy is to treat the right-hand side of the stream power equation as a generic nonlinear operator and apply a higher-order scheme for ordinary differential equations, such as a Runge-Kutta method.

## 9. Application to Transient River Profiles

[76] In this section, we analyze river profiles from a tectonically active environment in which uplift rates can vary in space and in time, and demonstrate how the analytical and semi-analytical solutions presented in previous sections assist in understanding the transient evolution of the profiles. The central Apennines in Italy contain a multitude of normal faults, many of which became active in Pliocene and Quaternary time. Here we examine the longitudinal elevation profiles of three rivers that cross three active normal faults in the central Apennines, all of which are thought to have become active at  $\sim 3$  Ma.

[77] The Rio Torto, Valleluce River, and Fosso Tascino were previously studied by Whittaker *et al.* [2007a, 2007b] and Attal *et al.* [2011]. Extensive field descriptions of these rivers already exist in the literature, such as in Whittaker *et al.* [2007a, 2007b]; the interested reader is referred to those papers for more detailed discussions of the field setting. We used the procedure described in section 4.2 to extract profiles and drainage areas from a 20 m resolution digital elevation map and identified the locations where the rivers cross normal faults based on the work of Whittaker *et al.* [2007a, 2007b]. It is noteworthy that these river profiles were extracted from

relatively noisy topographic data, giving rise to a roughness in the profiles that renders conventional slope-area analysis impractical. However, non-dimensionalization using the methods outlined in this paper renders the profiles suitable for modeling and interpretation of uplift histories.

[78] Thus far, we have assumed that climate, and precipitation rate in particular, does not change through time, so that all changes in non-dimensional slope are the result of temporal variations in uplift rate. It would instead be possible to choose temporal variations in precipitation rates in such a way that the non-dimensional river profiles are linear and can be explained by constant uplift rate. This is the equivalent of the observation that changes in concavity in dimensional river profiles can be due either to variations in uplift rate or climate. In the examples that follow, we assume that changes in concavity are due solely to variations in uplift rate.

### 9.1. Rio Torto

[79] The Fiamignano normal fault is thought to have become active at 3 Ma and to have had a slip rate of 0.30 mm/yr until  $\sim 750$  ka, when the slip rate in the central portion of the fault increased to 1.0 mm/yr [Roberts and Michetti, 2004; Whittaker *et al.*, 2007a, 2007b]. The Fiamignano fault is crossed by the Rio Torto, which, upstream from the fault, has a catchment area of 65 km<sup>2</sup>. Non-dimensionalization of the longitudinal profile results in a steep, linear downstream portion; a gently sloping, linear upstream portion; and a broad, concave-down section between the upstream and downstream portions (Figure 9a). The Fiamignano fault is located at the beginning of the dimensional and dimensionless profiles, at  $x = \chi = 0$ .

[80] The nonlinearity of this river profile indicates that the Rio Torto is not in steady state with respect to a constant rate of uplift. The profile is piecewise linear, however, suggesting partial adjustment of downstream reaches to the modern uplift rates and prior adjustment to an older episode of uplift revealed by the linear slope of the upstream reaches. In particular, the downstream steepening of the river profile at an elevation of  $\lambda \approx 400$ –500 is qualitatively consistent with the inferred increase in uplift rate from 0.3 mm/yr to 1.0 mm/yr. In this case, the concave-down section of the Rio Torto probably reflects the transition from a slower to faster uplift rate and corresponds to the concave-down stretch zones that typically form when  $n < 1$  (Figure 5).

[81] It is possible to fit the modern river profile of the Rio Torto using a range of values of  $n$ . Examples for  $n = 0.5$ ,  $n = 0.75$ , and  $n = 1.0$ , displayed in Figure 9, show that the downstream section of the river can be fit as having formed in response to a constant uplift rate while the upstream section can be fit as having formed in response to a constant but slower, uplift rate. For  $n = 0.5$ , we fit the dimensionless profile with an older uplift rate of  $v = 0.2$  followed by a more recent uplift rate of  $v = 0.7$  for a time  $\tau = 850$  (Table 2). If precipitation rates stayed approximately constant, then we can compare the modern rate to the older rate. In this case, the ratio of the modern rate to the older rate is 3.5, very similar to the change in rate inferred from geological studies of the Fiamignano fault [Roberts and Michetti, 2004; Whittaker *et al.*, 2007a, 2007b].

[82] If we instead use a value of  $n = 0.75$ , the fit to the observational profile data is only marginally worse. In this case, we fit the dimensionless profile with an older uplift rate

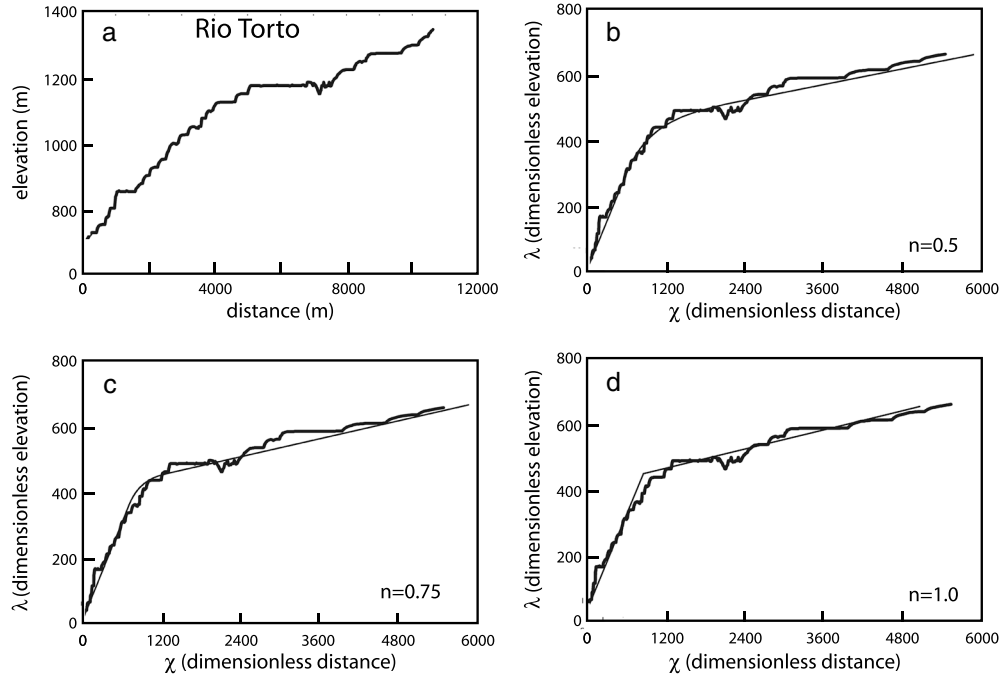


**Figure 9.** (a) Longitudinal profile for the Rio Torto. (b–d) Longitudinal profile for the Rio Torto in dimensionless variables (heavy line) and fits to the profile constructed using the slope patch method (light line). Rates of uplift are (b)  $v=0.2$  followed by an increase to  $v=0.7$  for a dimensionless time  $\tau=850$ , (c)  $v=0.1$  followed by an increase to  $v=0.6$  for a dimensionless time  $\tau=800$ , and (d)  $v=0.05$  followed by an increase to  $v=0.5$  for a dimensionless time  $\tau=900$

**Table 2.** Parameter Values Used for Example River Profiles<sup>a</sup>

Figure	Variable	Value(s)
1b (King Range)	$A_0$	$10^6 \text{ m}^2$
	$m/n$	0.4
9 and 10 (Apennines 1, Rio Torto)	$A_0$	$10^6 \text{ m}^2$
	$m/n$	0.40
9b and 10b	$n$	0.5, 0.75, 1.0
	$v$ ( $n=0.5$ )	0.7 (time <sup>1</sup> < 850) 0.2 (time <sup>1</sup> > 850)
9c	$v$ ( $n=0.75$ )	0.6 (time <sup>1</sup> < 800) 0.1 (time <sup>1</sup> > 800)
	$v$ ( $n=1.0$ )	0.5 (time <sup>1</sup> < 900) 0.05 (time <sup>1</sup> > 900)
11b (Apennines 2, Valletta River)	$A_0$	$10^6 \text{ m}^2$
	$m/n$	0.40
12 and 13 (Apennines 3, Fosso Tascino)	$n$	0.5, 0.75
	$v$ ( $n=0.5$ )	0.41
12c	$v$ ( $n=0.75$ )	0.26
	$A_0$	$10^6 \text{ m}^2$
12b	$m/n$	0.40
	$n$	0.5, 0.75
12c	$v$ ( $n=0.75$ )	0.18 (time <sup>b</sup> < 2100) 0.32 (time <sup>b</sup> > 2100)
	$v$ ( $n=0.5$ )	0.32 (time <sup>b</sup> < 2000) 0.47 (time <sup>b</sup> > 2000)
12d and 13b	$v$ ( $n=0.5$ )	0.32 (time <sup>b</sup> < 2900) 0.85 (2900 < time <sup>b</sup> < 3300) 0.47 (time <sup>b</sup> > 3300)

<sup>a</sup>For all dimensionless profiles, we use  $h_0 = 1 \text{ m}$  and  $r_0 = r(x) = 1 \text{ m}^{1-3m} \text{ yr}^{m-1}$ .

<sup>b</sup>Time denoted is dimensionless and is measured backwards from the present.

of  $v=0.1$  followed by a more recent uplift rate of  $v=0.6$  lasting for a time  $\tau=800$ . In this case, the ratio of the modern rate to the older rate is 6.0, approximately twice the increase in rate inferred from geological studies of the Fiamignano fault. If  $n$  is further increased to 1.0, the ratio of modern to older uplift rate is 10.0, nearly 3 times the rate inferred from geological studies. As  $n$  increases, this ratio increases, so that values of  $n$  significantly above 0.5 yield ratios that are incompatible with geological data [Roberts and Michetti, 2004; Whittaker *et al.*, 2007a, 2007b]. This suggests that  $n=0.5$  is a reasonable choice for this profile. Interestingly, this estimate for  $n$  is somewhat lower than values that have been used in previous investigations of the Rio Torto and similar Apennine rivers [Attal *et al.*, 2011], as well as values that have been estimated for other sites based on relationships between channel steepness and uplift rate [Kirby and Whipple, 2012].

[83] This example illustrates the power of the analytical methods developed in this paper and also illustrates that the precision of tectonic histories inferred from transient river profiles can depend on the quality of the topographic data and the uncertainty in the erosion parameters.

[84] The dimensionless curve that best approximates the longitudinal profile of the Rio Torto can also be computed at earlier times to simulate the possible history of the river. Figure 10 shows the evolution through time of one of the curves that provides a good fit to the Rio Torto, for  $n=0.5$  (Figure 9b), in dimensionless and dimensioned variables. The dimensionless and dimensioned profiles show similar patterns except that the dimensioned profiles are slightly concave up due to the effect of drainage area (which was assumed to be the same at all times) and that the upstream

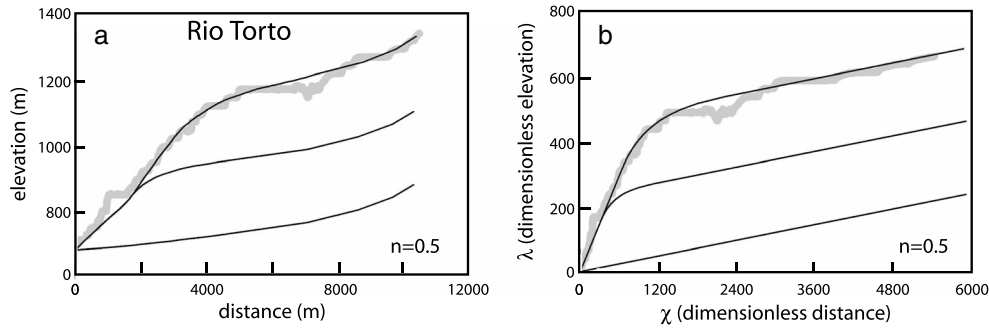


**Figure 10.** Time evolution inferred for the Rio Torto in dimensioned (a) and dimensionless (b) coordinates. In each panel, the model fits (thin black lines) to the observed river profile (thick gray line) are shown for the present day and two instants in the past separated by dimensionless time intervals  $\Delta\tau = 425$ . Model solution corresponds to that in Figure 9b.

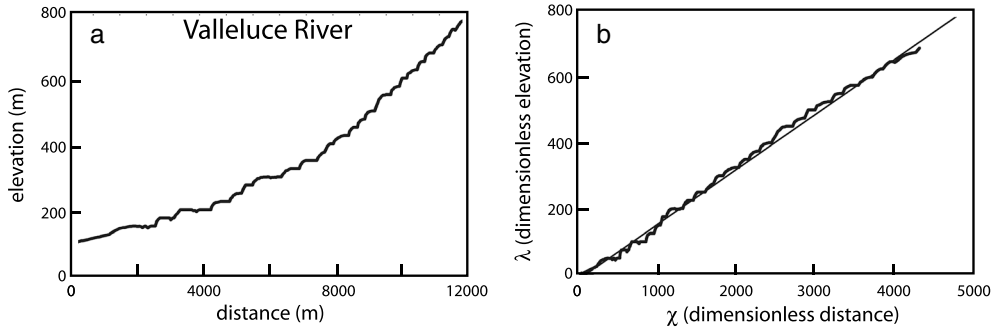


**Figure 11.** (a) Longitudinal profile for the Vallelluce River. (b) Longitudinal profile for the Vallelluce in dimensionless variables (heavy black line) and best linear fit (light gray line). For the slope shown, the dimensionless uplift rates are  $v = 0.41$  if  $n = 0.5$  and  $v = 0.26$  if  $n = 0.75$ .

portions of the river are expanded in the dimensionless case. The increase in uplift rate that has occurred for this river causes the upstream, gently sloping portions of the river to be uplifted relative to base level without significant change in slope. There is also a growing stretch zone between the steeper downstream and less steep upstream portions of the river.

## 9.2. Vallelluce River

[85] The South Cassino normal fault has a total throw of 1200 m. It is thought to have become active at 3 Ma and to have had a constant slip rate of 0.25–0.30 mm/yr [Roberts and Michetti, 2004; Whittaker et al., 2007b]. The South Cassino fault is crossed by the Vallelluce River which, upstream from the fault, has a drainage area of 20 km<sup>2</sup>. The river profile has a smooth, concave-up geometry (Figure 11a). The South Cassino fault is located at the beginning of the dimensional and dimensionless profiles, at  $x = \chi = 0$ . Non-dimensionalization of the longitudinal river profile reveals a linear profile with no difference in slope between upstream and downstream portions (Figure 11b). This indicates that the river profile is completely adjusted to the present rate of uplift, consistent with the independent inference that the South Cassino fault has experienced a roughly constant slip rate since 3 Ma.

[86] The Vallelluce River and the Rio Torto lie within the same region and traverse similar lithologies. We therefore

use the same values of  $n$  to interpret both profiles. For  $n = 0.5$ , the slope of the Vallelluce River corresponds to a dimensionless uplift rate of  $v = 0.41$ . This is slower than the modern rate of the Rio Torto by a factor of 1.6. For  $n = 0.75$ , the slope of the Vallelluce river corresponds to a dimensionless uplift rate of  $v = 0.26$ . This is slower than the modern rate of the Rio Torto by a factor of 2.3. Thus, the dimensionless profiles are consistent with the independent inference that the two rivers experienced somewhat similar uplift rates until ~750 ka, with Rio Torto's uplift rate subsequently quickening by roughly a factor of 3.

## 9.3. Fosso Tascino

[87] The Leonessa normal fault has a total throw of 1000 m. It is thought to have become active at 3 Ma and to have had a constant slip rate of 0.35 mm/yr [Roberts and Michetti, 2004; Whittaker et al., 2007a, 2007b]. The Leonessa fault is crossed by the Fosso Tascino, which, upstream from the fault, has a catchment area of 45 km<sup>2</sup>. The Leonessa fault is located at the beginning of the dimensional and dimensionless profiles, at  $x = \chi = 0$ . The longitudinal river profile is concave upwards with a pronounced steepening of the upstream portions of the profile (Figure 12a). Non-dimensionalization of the longitudinal river profile shows a profile that is piecewise linear with a more gently sloping downstream section and a steeper upstream section (Figures 12b–12d). The transition between sections corresponds to a concave-up knickpoint

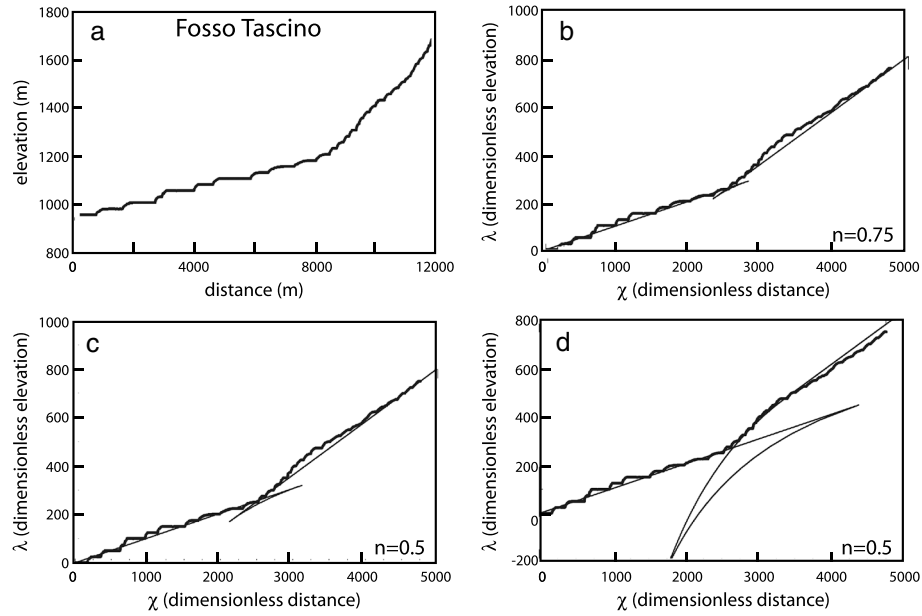


**Figure 12.** (a) Longitudinal profile for the Fosso Tascino. (b–d) Longitudinal profile for the Fosso Tascino in dimensionless variables (heavy black line) and fits to the profile constructed using the slope patch method (light gray line). Rates of uplift are (b)  $v=0.32$  followed by a decrease to  $v=0.18$  for a dimensionless time  $\tau=2100$ , (c)  $v=0.47$  followed by a decrease to  $v=0.32$  for a dimensionless time  $\tau=2000$ , and (d)  $v=0.47$  followed by an increase to  $v=0.85$  for a dimensionless time  $\tau=400$ , followed by a decrease to  $v=0.32$  for a dimensionless time  $\tau=2900$ .

(contrast with the non-dimensional profile for the Rio Torto in Figure 9b).

[88] We fit the non-dimensional profile of the Fosso Tascino using  $n=0.5$  and  $n=0.75$ . When  $n=0.5$ , this fit corresponds to an initial uplift rate of  $v=0.47$  followed by a decrease in rate to  $v=0.32$  for a dimensionless time  $\tau=2000$ . When  $n=0.75$ , this fit corresponds to an initial uplift rate of  $v=0.32$  followed by a decrease in rate to  $v=0.18$  for a dimensionless time  $\tau=2100$  (Table 2).

[89] Because the Fosso Tascino profile appears to contain a consuming knickpoint, information about previous episodes of uplift has been lost as individual slope patches disappeared into the knickpoint. It is impossible to recover the information lost into the knickpoint or even to determine how much information has been lost. For example, Figures 12b and 12c shows two possible fits to the observed profile where relatively little information is lost at the knickpoint, as evidenced by the small

size of the physically unrealized part of the profile. However, other very different fits can be made to the data with much greater loss of information. Figure 12d shows a very good fit to the lower linear river section and to the concave-up knickpoint (for  $n=0.5$ ) where the knickpoint is formed by interspersing the uplift rates computed for Figure 12c ( $v=0.32$  and  $0.47$ ) with a short period of very rapid uplift ( $v=0.85$  for a time interval  $\tau=400$ ) (Table 2). The large size of the physically unrealized portion of the profile indicates that much information has been lost to the knickpoint. In fact, all of the slope patches created in direct response to the very fast uplift rate have disappeared into the knickpoint, and there is effectively no remaining evidence that the period of rapid uplift occurred (Table 3).

[90] Inspection of Figure 12 sounds a cautionary note about how completely river profiles can be interpreted when they contain one or more migrating knickpoints. Many different scenarios are possible for a single value of  $n$ , with the differences disappearing into the knickpoints. This lack of uniqueness in reconstructing uplift histories occurs because of the loss of information into consuming knickpoints, so that the uplift record for some time intervals may no longer exist in the longitudinal river profile. This phenomenon is similar to the example given for oscillating uplift rates at base level: information about the size and nature of the oscillations disappears upstream, and the remaining signal reveals only the average rate of uplift (Figure 6). Interpretation of paleo-rivers, which lack a robust geological context, is particularly problematic [e.g., *Pritchard et al.*, 2009].

[91] One of the dimensionless curves that approximates the longitudinal profile of the Fosso Tascino can be computed over time to explore a possible history of the river. Figure 13 shows the evolution through time of the case  $n=0.5$

**Table 3.** Variables Used for Theoretical River Profiles

Figure	Variable	Value(s)
2	$n$	1.5
	$v$	2.0, 0.5
3	$n$	1.5
	$v$	2.0, 0.5
4	$n$	1.5
	$v$	0.5, 2.0
5	$n$	0.5, 1.0, 1.5
	$v$	0.5, 2.0, 0.5
6	$n$	0.5, 1.0, 1.5
	$v$	0.5, 2.0 alternating with period $T=4$
7	$n$	0.5, 1.5
	$v$	0.5 for $\chi < 2.5$ ; 2.0 for $\chi > 2.5$
8	$n$	1.0, 1.5
	$v$	4.0



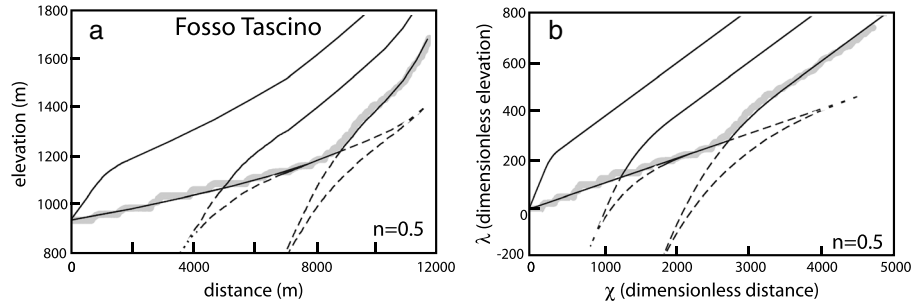


**Figure 13.** Time evolution inferred for the Fosso Tascino in dimensioned (a) and dimensionless (b) coordinates. In each panel, the model fits (thin black lines) to the observed river profile (thick gray line) are shown for the present day and two instants in the past separated by dimensionless time intervals  $\Delta\tau = 1450$ . Model solution corresponds to that in Figure 12d. The dashed black line indicates physically unrealized portions of the slope patch solution, which grow with time.

(Figure 12d). The decrease in uplift rate that occurred during development causes the downstream slope patches to over-ride the upstream slope patches at a migrating knickpoint. The triangular-shaped portions of the curve shown as dashed lines are the physically unrealized slope patches. This portion of the curve grows in time as information is progressively lost.

## 10. Discussion

### 10.1. Benefits of Non-Dimensionalization

[92] Non-dimensionalization of the stream power equation redefines the variable that designates horizontal position ( $x$ ) as a new variable ( $\chi$ ) that is proportional to the integral of upstream drainage area (with exponent  $-m/n$ ) integrated over the horizontal direction. This substitution produces a significant change in longitudinal elevation profiles that are plotted as a function of  $\chi$  because it removes the natural concavity of the profiles due to downstream increases in drainage area (Figure 1c). In the dimensionless format developed in this paper, the river gradient depends only on the uplift rate. The non-dimensionalization aids river profile analysis by helping to identify knickpoints and distinguish between different knickpoint types: stationary knickpoints associated with, for example, changes in bedrock erodibility or precipitation, are visible in dimensional profiles, but disappear in the dimensionless profiles.

[93] As demonstrated in section 9, this non-dimensionalization scheme also makes it possible to use poor quality or noisy topographic data to extract useful information about river profiles. Unlike the standard slope-area method, where differentiation of elevation data introduces additional noise, the non-dimensionalization method introduced here makes use of elevation data plotted against dimensionless distance to generate useful information about river evolution. In a separate paper [Perron and Royden, 2013], we provide a more detailed guide to performing the non-dimensionalization on river profiles extracted from topographic datasets and offer several examples that illustrate additional advantages over slope-area analysis.

### 10.2. Availability of Transient Analytical Solutions to the Stream Power Equation

[94] The stream power model (equations (1) and (8)), which is thought to describe the evolution of many rivers

incising into bedrock, is linear only in the special case where  $n = 1$ . In this instance, there is an exact analytical solution (section A). However, in the general nonlinear case, the equation has generally defied analytical solution (see Luke [1972] and Weissel and Seidl [1998] for previous analytical work). We have shown that slope patch analysis provides a natural means of generating analytical solutions to the nonlinear equation in several cases of interest, including the case where uplift rates vary in time or in space (but not both; equations (11)–(15), (D5), and (D6) and section B). In addition to providing insight into the behavior of evolving river profiles, these analytical solutions provide a powerful means of evaluating the accuracy of transient numerical solutions, which are frequently incorporated into landscape evolution models in one and two dimensions.

### 10.3. Preservation and Destruction of Information in Transient River Profiles

[95] Slope patches are mathematical entities that carry information about downstream river states, such as the rate of uplift relative to base level. They travel upstream at a rate that depends on the slope of the patch and on the local uplift rate. Information cannot travel upstream faster than the slope patch that carries it. Slope patches also form contiguous “stretch zones” where all the slope patches in the zone grow out of a single instant in time at base level and stretch apart during upstream migration. Stretch zones have characteristic curvature diagnostic of  $n$ . For  $n < 1$ , stretch zones are concave down, and for  $n > 1$ , stretch zones are concave up.

[96] Unless  $n = 1$ , slope patches disappear into migrating knickpoints from both the upstream and downstream sides of the knickpoint (Figure 5). The information carried by the disappearing slope patches is also lost, so that the longitudinal river profile does not contain complete information about past river states. Because information is lost at migrating knickpoints, reconstruction of uplift histories from river profiles may be problematic unless the erosional parameters, the value of  $n$ , and the geological parameters are well known, a topic we explore further in section 10.4. This is particularly so for profiles where it is difficult to distinguish migrating knickpoints from tightly defined stretch zones and where it is difficult to tell which part of the uplift history has been destroyed (at migrating knickpoints) and which part has been preserved.

#### 10.4. Not All Knickpoints Are Created Equal

[97] Our analysis provides a theoretical framework for understanding two distinct types of knickpoint that can develop along river profiles. Stationary knickpoints exist over regions where there is a lateral change in uplift rate (section D and Figure 8). Slope patches do not disappear at stationary knickpoints, which may be concave up or down for any value of  $n$ . Slope patches migrate across stationary knickpoints and change their slope as they do so. Accordingly, no information about past river states is lost at stationary knickpoints. All migrating knickpoints are consuming knickpoints (unless  $n=1$ ). They differ from stationary knickpoints not only in their upstream propagation and ability to absorb adjacent slope patches, but also because they are not symmetrically developed. For  $n > 1$ , migrating knickpoints can be maintained only when they are concave down, while the converse is true for  $n < 1$  (Figure 5).

[98] In short, our analysis demonstrates that some knickpoints are related to local changes in uplift rate or erosional efficiency while others reflect propagation of transient features upstream and that some knickpoints preserve information while others destroy it. The possibility that more than one type of knickpoint may be present on a river profile [Crosby and Whipple, 2006] presents a challenge for the interpretation of paleo-river profiles or any river profiles where knickpoints are present and geologic data are not available to constrain the location and nature of uplift along the profile. This was illustrated in Figures 12c and 12d, where two significantly different uplift histories can be used to fit the upstream river profiles of the Fosso Tascino river. The uncertainty lies in what and how much information has been lost at the migrating knickpoint. Any time knickpoints are present in longitudinal river profiles, great care must be taken to ascertain the type of knickpoint and the end-member conditions for information loss.

[99] As noted in section 2, our analysis does not explicitly account for additional factors that can influence knickpoint migration and morphology, such as rock fracture patterns [Lamb and Dietrich, 2009], inhibition or enhancement of erosion by sediment [Whipple and Tucker, 2002], flow and lithologic controls on channel cross-sectional geometry [Lavé and Avouac, 2001; Montgomery and Gran, 2001; Duvall et al., 2004], or the interplay of erosion thresholds and variable water discharge [Tucker, 2004; Lague et al., 2005; Molnar et al., 2006; DiBiase and Whipple, 2011]. A detailed consideration of how these various factors influence transient river profile evolution is beyond the scope of this paper. Instead, we have adopted the general formulation in equations (1) and (2), which subsumes such effects in a spatially variable erosion coefficient,  $r$ . In the examples presented here, we have explored the implications of the simplest bedrock channel incision model that is commonly used to describe the long-term dynamics of many channels. However, our approach is sufficiently general that it can incorporate other components, potentially including mechanisms that are not currently appreciated, provided they can be cast as separable functions of downstream distance and time. Even if these functions cannot be expressed in simple analytical form, our slope patch solution method can be applied numerically, tracing the propagation, preservation, or destruction of information in river profiles in a way that is not possible with conventional numerical solutions.

#### 10.5. Constraints on the Slope Exponent $n$

[100] The slope exponent  $n$  is one of the crucial parameters that control the evolution of bedrock rivers governed by the stream power equation, but determining  $n$  is not easy. The analysis presented in this paper suggests several methods for constraining the range of possible values for  $n$ . First, the ratio of dimensionless slopes of two similar rivers undergoing different rates of base level uplift is equal to the ratio of their rates of uplift raised to the power  $\frac{1}{n}$ , provided their precipitation rates and erodibilities are equal. If the dimensionless slopes are well determined, and the ratios of erodibilities, precipitation rates, and rates of uplift are known independently, then there may be only a limited range of  $n$  that will satisfy the slope data and the uplift data. A similar approach can be used with conventional slope-area analysis, but this requires an estimate of the ratio of the slope intercepts for the two profiles, which are usually less well constrained than the slopes of the dimensionless profiles in our analysis.

[101] A second method that can be used is the identification of migrating (consuming) knickpoints, which will indicate whether  $n$  is greater or less than 1. If migrating knickpoints are concave down, then  $n$  must be greater than one. If migrating knickpoints are concave up, then  $n$  must be less than 1. Tucker and Whipple [2002] demonstrated this distinction with numerical solutions for the transient relaxation of a river profile from an initial step.

[102] Third, broadly curved regions of a profile that we have called “stretch zones,” which are effectively the opposite of knickpoints, can be interpreted to have grown out of a nearly instantaneous change in uplift rate (from slow to fast if  $n < 1$  and fast to slow if  $n > 1$ ). If this is the case, the curvature of the profile can be used to constrain the probable range of  $n$ , as was done for the Fosso Tascino (Figures 12b and 12c).

### 11. Conclusions

[103] We present a new approach to understanding and evaluating the behavior of longitudinal river profiles in both steady state and transient phases of evolution. This approach offers several new insights into the evolution of bedrock rivers. First, longitudinal river profiles can be non-dimensionalized in a way that removes the effects of drainage area from the stream power equation. Under this formulation, river profiles in steady state become linear. Second, non-dimensionalization makes it possible to derive analytical solutions for the transient evolution of river profiles that are governed by the stream power equation. Third, river profiles evolve through the upslope migration of “slope patches,” which carry topographic information upstream. For spatially uniform uplift rates, the slope of these patches does not change with time.

[104] Fourth, slope patches travel upstream at a rate that depends only the slope of the patch and the slope exponent,  $n$ . “Stretch zones” are created when slope patches diverge, and “consuming knickpoints” are created when slope patches overtake one another. Fifth, the behaviors of longitudinal river profiles demonstrated in this paper highlight the different roles carried out by migrating and stationary knickpoints. All migrating knickpoints are consuming knickpoints, and information about past river states is progressively lost at migrating knickpoints. This loss of information imposes a fundamental limit

on reconstructions of uplift histories based on river profiles. Together, the methods of non-dimensionalization and slope patch analysis provide powerful new tools for understanding the transient behavior of bedrock rivers.

### Appendix A: General Analytical Solution for the Case $n=1$

[105] For the case where  $n=1$ , the slope patch solutions (equations (10)–(13), (D3), and (D4)) are considerably simplified. Because  $n=1$  yields a linear stream power equation (equation 8), it is possible to find an ordinary general solution to this equation. Consider an arbitrary initial stream profile with base level maintained at  $\chi=0$ ,  $\lambda=0$  and initial topography defined at time  $\tau=0$ :

$$\begin{aligned} \lambda_{\text{initial}} &= \lambda(\chi, 0) & \chi &\geq 0 \\ \lambda_{\text{initial}} &= 0 & \chi &< 0 \end{aligned} \quad (\text{A1})$$

[106] For uplift rates that are an arbitrary function of space and time, define

$$\begin{aligned} v(\chi, \tau) &= v(\chi, \tau) & \chi &\geq 0 \\ v(\chi, \tau) &= 0 & \chi &< 0 \end{aligned} \quad (\text{A2})$$

[107] Then the general solution to the river profile evolution equation (8) is

$$\lambda(\chi, \tau) = \lambda(\chi - \tau, 0) + \int_{\chi-\tau}^{\chi} v(\chi', (\chi' - \chi + \tau)) d\chi' \quad (\text{A3})$$

[108] All problems involving the evolution of river profiles with  $n=1$  can be solved by analytical or numerical computation of the integral in equation (A3). For many problems of interest, this integral may be computed analytically.

[109] When uplift is temporally invariant, the general solution simplifies to

$$\lambda(\chi, \tau) = \lambda(\chi - \tau, 0) + \int_{\chi-\tau}^{\chi} v(\chi') d\chi' \quad (\text{A4})$$

[110] When uplift is spatially invariant uplift, we make the substitution

$$\tau' = \chi' - \chi + \tau \quad (\text{A5})$$

into equation (A3) and simplify to obtain

$$\lambda(\chi, \tau) = \lambda(\chi - \tau, 0) + \int_0^{\tau} v(\tau') d\tau' \quad (\text{A6})$$

[111] Under temporally invariant uplift (equation (A4)), the time required for a segment of river located at position  $\chi$  to reach steady state is  $\tau = \chi$ . At this point, the river segment no longer has any memory of the initial river profile. Rivers with temporally varying uplift rates (equations (A3) and (A6)) do not, in general, reach steady state. Nevertheless, in this case, the time for a segment of river located at

position  $\chi$  to lose all memory of the initial river profile is also  $\tau = \chi$ .

## Appendix B

### B1. Derivation of Solution for Spatially Invariant Uplift Rate

[112] In order to derive a solution for the case where uplift is spatially invariant, we track the motion of individual slope patches during upstream migration. Base level is set at  $\chi=0$  and  $\lambda=0$ , and the river exists only for positive values of  $\chi$ .

[113] Consider the case of uplift at a constant and uniform rate  $v(\tau_i)$  between times  $\tau_{i-1}$  and  $\tau_i$ . The slope of the patch is set by the steady state solution to equation (8) for erosion at a rate  $v(\tau_i)$ :

$$\frac{d\lambda}{d\chi} = v(\tau_i)^{1/n} \quad (\text{B1})$$

[114] By time  $\tau_i$ , this results in a short segment of steady state river profile whose surface position is given by the steady state solution to equation (8):

$$\lambda(\chi, \tau_i) = \chi [v(\tau_i)]^{1/n} \quad (\text{B2})$$

[115] At time  $\tau_i$ , the uplift rate changes to  $v(\tau_{i+1})$  and remains constant until time  $\tau_{i+1}$ . This results in a new steady state river segment at the downstream end of the river, while the slope patch generated between  $\tau_{i-1}$  and  $\tau_i$  continues to migrate upstream. The older slope patch is modified by undergoing erosion at a rate  $v(\tau_i)$ ; it is also uplifted with the bedrock at  $v(\tau_{i+1})$ . Thus, at time  $\tau_{i+1}$ , the elevation of this older slope patch is given by

$$\lambda(\chi, \tau_{i+1}) = \chi [v(\tau_i)]^{1/n} + (\tau_{i+1} - \tau_i) [v(\tau_{i+1}) - v(\tau_i)] \quad (\text{B3})$$

[116] Now consider some later time  $\tau_f$ . The steady state river segment that formed between time  $\tau_{i-1}$  and  $\tau_i$  (equation (B1)) has continued to erode at a rate  $v(\tau_i)$ , to give a total amount of erosion  $[v(\tau_i)(\tau_f - \tau_i)]$ . At the same time, the bedrock has been uplifted by an amount equal to the integral of uplift rate between time  $\tau_i$  and time  $\tau_f$ . This yields an elevation for this section of river at time  $\tau_f$  of

$$\lambda(\chi, \tau_f) = \chi [v(\tau_i)]^{1/n} + \int_{\tau_i}^{\tau_f} [v(\tau') - v(\tau_i)] d\tau' \quad (\text{B4})$$

[117] Similarly, the younger steady state river segment that formed between time  $\tau_i$  and  $\tau_{i+1}$  (equation (B2)) has an elevation at time  $\tau_f$  of

$$\lambda(\chi, \tau_f) = \chi [v(\tau_{i+1})]^{1/n} + \int_{\tau_{i+1}}^{\tau_f} [v(\tau') - v(\tau_{i+1})] d\tau' \quad (\text{B5})$$

[118] The intersection of these two steady state river segments also migrates upstream with time, and the elevation and lateral position of this intersection point can be computed at any time by equating the right-hand sides of

equations (B4) and (B5). Re-arranging and canceling terms inside the integrals yields

$$[v(\tau_{i+1}) - v(\tau_i)](\tau_f - \tau_i) + \int_{\tau_i}^{\tau_{i+1}} [v(\tau') - v(\tau_{i+1})] d\tau' = \chi \left\{ [v(\tau_{i+1})]^{\frac{n-1}{n}} - [v(\tau_i)]^{\frac{n-1}{n}} \right\} \quad (B6)$$

[119] Dividing by  $[v(\tau_{i+1}) - v(\tau_i)]$  and taking the limit as  $(\tau_{i+1} - \tau_i)$  goes to zero and re-arranging, we find

$$\chi = n v(\tau_i)^{\frac{n-1}{n}} (\tau_f - \tau_i) \quad (B7)$$

[120] And finally, substitute  $\chi$  back in to equation (B4) to solve for elevation

$$\lambda(\chi, \tau_f) = (n-1)v(\tau_i)(\tau_f - \tau_i) + \int_{\tau_i}^{\tau_f} v(\tau') d\tau' \quad (B8)$$

## B2. Proof of Solution for Spatially Invariant Uplift Rate

[121] It is not difficult to show that equations (B7) and (B8) are solutions to the stream power equation (8) by taking the derivative of  $\lambda$  with respect to  $\chi$  at fixed  $\tau$  and the derivative of  $\lambda$  with respect to  $\tau$  at fixed  $\chi$ . For fixed  $\tau$ ,

$$\left. \frac{\partial \lambda}{\partial \chi} \right|_{\text{fixed } \tau} = \frac{\partial \lambda}{\partial \tau_i} \frac{\partial \tau_i}{\partial \chi} \quad (B9)$$

[122] Differentiating equation (B8) with respect to  $\tau_i$

$$\frac{\partial \lambda}{\partial \tau_i} = -nv(\tau_i) + (n-1)(\tau - \tau_i) \left. \frac{\partial v}{\partial \tau} \right|_{\tau_i} \quad (B10)$$

and differentiating equation (B7) with respect to  $\chi$

$$1 = \left[ -nv(\tau_i)^{\frac{n-1}{n}} + (n-1)(\tau - \tau_i) v(\tau_i)^{-1/n} \left. \frac{\partial v}{\partial \tau} \right|_{\tau_i} \right] \frac{\partial \tau_i}{\partial \chi} \quad (B11)$$

yields

$$\frac{\partial \lambda}{\partial \tau_i} \frac{\partial \tau_i}{\partial \chi} = \frac{-nv(\tau_i) + (n-1)(\tau - \tau_i) \left. \frac{\partial v}{\partial \tau} \right|_{\tau_i}}{-nv(\tau_i)^{\frac{n-1}{n}} + (n-1)(\tau - \tau_i) v(\tau_i)^{-1/n} \left. \frac{\partial v}{\partial \tau} \right|_{\tau_i}} \quad (B12)$$

[123] Simplifying the fraction and substituting into equation (B9) gives

$$\left. \frac{\partial \lambda}{\partial \chi} \right|_{\text{fixed } \tau} = v(\tau_i)^{1/n} \quad (B13)$$

[124] Following a similar procedure but differentiating equation (B8) with respect to  $\tau$ , we find that at fixed  $\chi$ ,

$$\left. \frac{\partial \lambda}{\partial \tau} \right|_{\text{fixed } \chi} = (n-1)v(\tau_i) + v(\tau) + \left[ -nv(\tau_i) + (n-1)(\tau - \tau_i) \left. \frac{\partial v(\tau_i)}{\partial \tau_i} \right] \frac{\partial \tau_i}{\partial \tau} \quad (B14)$$

and differentiating equation (B7) with respect to  $\tau_i$  at fixed  $\chi$ ,

$$0 = \left[ n v(\tau_i)^{(n-1)/n} \right] \frac{\partial \tau}{\partial \tau_i} - n v(\tau_i)^{\frac{n-1}{n}} + (n-1)(\tau - \tau_i) v(\tau_i)^{-1/n} \frac{\partial v(\tau_i)}{\partial \tau_i} \quad (B15)$$

[125] Equations (B15) and (B16) can be combined to eliminate the time derivatives in  $\tau$  and  $\tau_i$  and simplify to

$$\left. \frac{\partial \lambda}{\partial \tau} \right|_{\text{fixed } \chi} = v(\tau) - v(\tau_i) \quad (B16)$$

[126] By inspection, equations (B14) and (B16) together provide a solution to the stream power equation (8) for spatially invariant uplift.

## B3. Solution for Spatially Invariant Uplift Rate with Initial Elevation

[127] If there is an initial elevation consisting of elevations  $\lambda_i$  at positions  $\chi_i$ , then we must also consider the behavior of slope patches that are already present at time zero (thus,  $\tau_i = 0$ ). Therefore, we rewrite the solution given in equations (B7) and (B8) by setting  $\tau_i$  to zero but including the initial position and elevation terms. We also make the substitution  $v_i = \sigma_i^n$  so that for slope patches that are present in the initial elevation profile, the solution will be in terms of the initial slope of the patch rather than the initial uplift rate that generated the patch. This yields

$$\chi - \chi_i = n \sigma_i^{n-1} \tau_f \quad (B17)$$

and

$$\lambda - \lambda_i = (n-1)\sigma_i^n \tau_f + \int_0^{\tau_f} v(\tau') d\tau' \quad (B18)$$

[128] These can be shown to comprise a valid solution in the same way as above.

## Appendix C: Numerical Implementation: Time-Invariant Uplift Rates

[129] Theoretical river profiles can be constructed numerically for temporally varying, spatially invariant, uplift rates by first defining an “initial” profile. In dimensionless coordinates, this profile consists of paired points  $(\chi, \lambda)$  which can be used to compute the slope at each point. This dimensionless slope is the slope of a “slope patch” at each point. The patch will migrate upstream at a rate determined only by its slope. The patch is then allowed to migrate upstream over a succession of time steps, with the recursion algorithm for horizontal and vertical positions being

$$\chi_{\text{new}} = \chi_{\text{old}} + n \sigma^{n-1} \Delta \tau \quad (C1)$$

$$\lambda_{\text{new}} = \lambda_{\text{old}} + (n-1)\sigma^n \Delta \tau + v \Delta \tau \quad (C2)$$

[130] These equations are the equivalent of equations (11) and (12) in the main text.

[131] In the case where the uplift rates are spatially invariant, the dimensionless slope of each slope patch,  $\sigma$ , remains constant throughout the computation. New slope patches are generated at base level with a slope that depends only on the uplift rate and on the slope exponent,  $n$ . These have a

horizontal and vertical position of zero in the time step when they are first generated and a slope

$$\sigma = v^{1/n} \quad (C3)$$

[132] This equation is the equivalent of equation (13) in the main text.

[133] The patch is then allowed to migrate up the river as given by equations C1 and C2. Care must be taken when changing uplift rates to make uplift rate a smooth function of time. In practice, the easiest method is to generate a number (such as 10 or 20) of slope patches at base level every time there is a change in uplift rate and assign each patch a different slope such that the points interpolate between the slope corresponding to the “new” uplift rate and the slope corresponding to the “old” uplift rate. It is out of these points that the stretch zones and consuming zones will develop and these extra points are needed to obtain sufficient resolution and smoothness in these parts of the curve.

[134] For spatially varying uplift rates, the computational procedure is nearly the same except that the slope of each patch may change with time as the patch migrates from a region of faster uplift to slower uplift or vice versa. The recursion algorithms in equations (C1) and (C2) need to be replaced by the equivalent equations (D5) and (D6). The slope of each patch is given by equation (D3) and needs to be re-evaluated every time step. For spatially variable rates of uplift, the initial distribution of slope patches and river gradients must be made with care. For example, the rate at which slope patches migrate over a zero-gradient section of river is either zero or infinite, depending on whether  $n$  is greater than or less than 1. Hence, exactly zero river gradients pose special problems in implementation, although the use of low-slope but effectively zero gradients can solve this problem. One also needs to be sure that the initial supply of slope patches is sufficient to delineate the evolving river profiles as sometimes the distance between slope patches traveling at different rates can become too large.

## Appendix D: River Profiles for Time-Invariant Uplift Rates

[135] Here we discuss the case in which uplift rates vary spatially but not temporally and in which the river profile may have nonzero initial elevations. Such a profile will consist partially of slope patches that already existed at positions  $\chi_i$  at initial time  $\tau = 0$  and partially of slope patches that are generated at the base of the river at a later time  $\tau_i$ .

### D1. Behavior of Slope Patches

[136] Consider a slope patch that exists at time  $\tau_i$  with a slope  $\sigma = \partial \lambda / \partial \chi$ . The bedrock uplift rate beneath the slope patch is  $v_i$ . There is a net upward motion of the bedrock surface at a rate given by equation (8), which we rewrite slightly as

$$\frac{\partial \lambda}{\partial \tau} = v(\chi_i, \tau_i) - \sigma(\chi_i, \tau_i)^n \quad (D1)$$

[137] At time  $\tau_{i+1}$ , the leading edge of this slope patch migrates upstream into a region with bedrock uplift rate of

$v_{i+1}$ . On the leading edge of the surface patch, there is a rate of vertical motion of the bedrock surface equal to

$$\frac{\partial \lambda}{\partial \tau} = v(\chi_{i+1}, \tau_{i+1}) - \sigma(\chi_{i+1}, \tau_{i+1})^n \quad (D2)$$

[138] Because the surface patch must be continuous across the boundary between the two areas of different uplift rate, the two rates of motion of the basement surface must be equal. Re-arranging slightly and generalizing, we obtain

$$\sigma(\chi)^n - v(\chi) = \sigma(\chi_i, \tau_i)^n - v(\chi_i, \tau_i) \quad (D3)$$

[139] The right-hand side of this equation is a constant, so that there is a kind of conservation principle for slope patches: their slope to the power of  $n$  is equal to the local uplift rate of the underlying basement plus a constant. Re-arranging, we obtain an expression for the slope of the patch as it migrates across regions of spatially varying uplift.

$$\sigma(\chi) = [\sigma(\chi_i, \tau_i)^n - v(\chi_i, \tau_i) + v(\chi)]^{1/n} \quad (D4)$$

[140] When the slope patch is generated at base level, the patch is in steady state with the rate of uplift at base level. The terms dependent on  $\chi_i$  (right-hand side of equation (D4)) cancel, and the slope of the patch is equal to the local uplift rate to the power  $\frac{1}{n}$ . In this case, the slope patch is always in steady state with respect to the underlying uplift.

[141] The rate at which a slope patch migrates horizontally depends only on the slope of the patch, as was shown for the case of spatially invariant uplift in equation (14). Substituting into equation (14) the expression for slope from equation (D4), we obtain

$$\frac{\partial \chi}{\partial \tau} = n [\sigma(\chi_i, \tau_i)^n + v(\chi) - v(\chi_i, \tau_i)]^{\frac{n-1}{n}} \quad (D5)$$

[142] Similarly, substituting the expression for slope into equation (15) for the vertical rate of slope patch migration gives

$$\frac{\partial \lambda}{\partial \tau} = (n-1)[\sigma(\chi_i, \tau_i)^n + v(\chi) - v(\chi_i, \tau_i)] + v(\chi) \quad (D6)$$

[143] Equations (D4)–(D6) are valid for surface patch migration for patches already in place at an initial time (in which case  $\tau_i = 0$ ) and also for patches generated later at base level (in which case  $\chi_i = 0$ ). These equations are sufficient to compute an evolving river profile for the case of temporally invariant uplift rates by time stepping through the profile evolution.

### D2. Time Scales to Develop Steady State River Profiles

[144] Rivers subjected to time-invariant uplift rates will always reach a steady state elevation profile given sufficient time. Inspection of equation (8) shows that the steady state elevation profile for a region uplifted at  $v(\chi)$  is

$$\lambda = \int_0^\chi d\chi' v(\chi')^{1/n} \quad (D7)$$

[145] In dimensionless format, steady state profiles have uniform gradients over regions of spatially uniform uplift rate. Spatial variations in steady state river gradients correspond to

spatial variations in uplift rate. Stationary knickpoints are present wherever uplift rates change abruptly along the river, such as across active faults.

[146] Although steady state river profiles do not change their shape as a function of time, they also consist of slope patches that migrate upstream with time. Steady state slope patches travel upstream along the steady state elevation profile, with the slope of each patch changing as it crosses regions subjected to different rates of uplift. Thus, we can use the rate at which slope patches migrate up the steady state profile to constrain the time needed to achieve steady state. For example, if we consider a river elevation profile that, at time  $\tau_1$ , is in steady state downstream of position  $\chi_1$  and out of steady state from  $\chi_1$  to  $\chi_2$ , then re-arranging and integrating equation (D5) gives the time that it takes a steady state slope patch initially at  $\chi_1$  to travel to  $\chi_2$ :

$$(\tau_2 - \tau_1) = \frac{1}{n} \int_{\chi_1}^{\chi_2} d\chi' v(\chi')^{(1-n)/n} \quad (\text{D8})$$

[147] This is a minimum bound on the time needed to reach steady state and applies to the case in which the migrating slope patch in question does not disappear upstream into a migrating knickpoint. When a migrating knickpoint is present in the interval from  $\chi_1$  to  $\chi_2$ , steady state will not be established until some slope patch that passes through position  $\chi_1$  at some time equal to or later than  $\tau_1$  migrates up the steady state profile and reaches  $\chi_2$  while remaining part of the physically realized solution.

[148] Thus, equations (19) and (D8) give the basic time scales for a river to abandon a former equilibrium state and to reach a new equilibrium state after a change in uplift rate.

[149] **Acknowledgments.** We thank Kelin Whipple for stimulating interest in the stream power equation and its implications and Brendan Meade for discussions of numerical methods for river profile evolution, and John Diniz for stimulating the revival of this project. This work was supported by the NSF Geomorphology and Land-use Dynamics Program under award EAR-0951672 to J.T.P. and by the Continental Dynamics Program under award EAR-0003571 to L.R. We thank Dmitri Lague, Alex Whittaker, and two anonymous reviewers for suggestions that helped us improve the paper.

## References

- Attal, M., P. A. Cowie, A. C. Whittaker, D. Hopley, G. E. Tucker, and G. P. Roberts (2011), Testing fluvial erosion models using the transient response of bedrock rivers to tectonic forcing in the Apennines, Italy, *J. Geophys. Res.*, **116**, F02005, doi:10.1029/2010JF001875.
- Beaumont, C., P. Fullsack, and J. Hamilton (1992), Erosional control of active compressional orogens, in *Thrust Tectonics*, edited by K. R. McClay, pp. 1–18, Chapman Hall, New York.
- Crosby, B.T., and K.X. Whipple (2006), Knickpoint initiation and distribution within fluvial networks: 236 waterfalls in the Waipaoa River, North Island, New Zealand, *Geomorphol.*, **82**, 16–38, doi:10.1016/j.geomorph.2005.08.023.
- DiBiase, R. A., and K. X. Whipple (2011), The influence of erosion thresholds and runoff variability on the relationships among topography, climate, and erosion rate, *J. Geophys. Res.*, **116**, F04036, doi:10.1029/2011JF002095.
- Duvall, A., E. Kirby, and D. W. Burbank (2004), Tectonic and lithologic controls on channel profiles and processes in coastal California, *J. Geophys. Res.*, **109**, F03002, doi:10.1029/2003JF000086.
- Finnegan, N.J., G. Roe, D. R. Montgomery, and B. Hallet (2005), Controls on the channel width of rivers: Implications for modeling fluvial incision of bedrock, *Geology*, **33**, 229–232, doi:10.1130/G21171.1.
- Finnegan, N.J., L.S. Sklar, and T.K. Fuller (2007), The interplay of sediment supply, river incision and bedrock channel morphology revealed by the transient evolution of an experimental bedrock channel, *J. Geophys. Res.*, **112**, F03S11, doi:10.1029/2006JF000569.
- Howard, A. D., and G. Kerby (1983), Channel changes in badlands, *Bull. Geol. Soc. Am.*, **94**(6), 739–752.
- Howard, A. D. (1994), A detachment-limited model of drainage basin evolution, *Water Res. Res.*, **30**(7), 2261–2286.
- Howard, A. D., W. E. Dietrich, and M. A. Seidl (1994), Modeling fluvial erosion on regional to continental scales, *J. Geophys. Res.*, **99**(B7), 13,971–13,986.
- Kirby, E., and K. X. Whipple (2012), Expression of active tectonics in erosional landscapes, *J. Structural Geol.*, **44**, 54–75, doi:10.1016/j.jsg.2012.07.009.
- Lague, D., N. Hovius, and P. Davy (2005), Discharge, discharge variability, and the bedrock channel profile, *J. Geophys. Res.*, **110**, F04006, doi:10.1029/2004JF000259.
- Lamb, M. P., and W. E. Dietrich (2009), The persistence of waterfalls in fractured rock, *Geol. Soc. Am. Bull.*, **121**, 1123–1134, doi:10.1130/B26482.1.
- Lavé, J., and J. P. Avouac (2001), Fluvial incision and tectonic uplift across the Himalayas of central Nepal, *J. Geophys. Res.*, **106**, 26,561–26,591.
- Luke, J. C. (1972), Mathematical models of landform evolution, *J. Geophys. Res.*, **77**, 2,460–2,464.
- Luke, J. C. (1974), Special solutions for nonlinear erosion problems, *J. Geophys. Res.*, **79**, 4035–4040.
- Luke, J. C. (1976), A note on the use of characteristics in slope evolution models, *Z. Geomorph. Supp.*, **25**, 114–119.
- Merritts, D., and K.R. Vincent (1989), Geomorphic response of coastal streams to low, intermediate, and high rates of uplift, Medocino triple junction region, northern California, *Geol. Soc. Am. Bull.*, **101**(11), 1373–1388.
- Merritts, D., and W. B. Bull (1989), Interpreting Quaternary uplift rates at the Mendocino triple junction, northern California, from uplifted marine terraces, *Geology*, **17**(11), 1020–1024.
- Molnar, P., R. S. Anderson, G. Kier, and J. Rose (2006), Relationships among probability distributions of stream discharges in floods, climate, bed load transport, and river incision, *J. Geophys. Res.*, **111**, F02001, doi:10.1029/2005JF000310.
- Montgomery, D. R., and K. B. Gran (2001), Downstream variations in the width of bedrock channels, *Water Resour. Res.*, **37**, 1841–1846.
- Nelson, P. A., and G. Seminara (2011), Modeling the evolution of bedrock channel shape with erosion from saltating bed load, *Geophys. Res. Lett.*, **38**, L17406, doi:10.1029/2011GL048628.
- Perron, J. T., and L. Royden (2013), An integral approach to bedrock river profile analysis, *Earth Surf. Process. Landforms*, in press, doi:10.1002/esp.3302.
- Pritchard, D., G. G. Roberts, N. J. White, and C. N. Richardson (2009), Uplift histories from river profiles, *Geophys. Res. Lett.*, **36**, L24301, doi:10.1029/2009GL040928.
- Roberts, G.P., and A.M. Michetti (2004), Spatial and temporal variations in growth rates along active normal fault systems: An example from Lazio-Abruzzo, central Italy, *J. Struct. Geol.*, **26**, 339–376, doi:10.1016/S0191-8141(03)00103-2.
- Rosenbloom, N. A., and R. S. Anderson (1994), Hillslope and channel evolution in a marine terraced landscape, Santa Cruz, California, *J. Geophys. Res.*, **99**(B7), 14,013–14,029.
- Seidl, M. A., and W. E. Dietrich (1992), The problem of channel erosion into bedrock, *Catena*, **23**(D24), 101–124.
- Seidl, M. A., W. E. Dietrich, and J. W. Kirchner (1994), Longitudinal profile development into bedrock: An analysis of Hawaiian channels, *J. Geol.*, **102**(4), 457–474.
- Sklar, L. S., and W. E. Dietrich (1998), River longitudinal profiles and bedrock incision models: Stream power and the influence of sediment supply, in *Rivers Over Rock*, edited by J. Tinkler, and E. Wohl, pp. 237–260, Geophysical Monograph 107, American Geophysical Union, Washington, D.C.
- Sklar, L., and W. E. Dietrich (2001), Sediment supply, grain size and rock strength controls on rates of river incision into bedrock, *Geology*, **29**, 1087–1090.
- Sklar, L.S., and W. E. Dietrich (2004), A mechanistic model for river incision into bedrock by saltating bedload, *Water Resour. Res.*, **40**, W06301, doi:10.1029/2003WR002496.
- Sklar, L.S., and W.E. Dietrich (2008), Implications of the saltation-abrasion bedrock incision model for steady state river longitudinal profile relief and concavity, *Earth Surf. Process. Landforms*, doi:10.1002/esp.1689.
- Snyder, N. P., K. X. Whipple, G. E. Tucker, and D. J. Merritts (2000), Landscape response to tectonic forcing: Digital elevation model analysis of stream profiles in the Mendocino triple junction region, northern California, *GSA Bull.*, **112**(8), 1250–1263.
- Snyder, N. P., K. X. Whipple, G. E. Tucker, and D. J. Merritts (2003), Importance of a stochastic distribution of floods and erosion thresholds

- in the bedrock river incision problem, *J. Geophys. Res.*, 108(B2), 2117, doi:10.1029/2001JB001655.
- Spiegelman, M., and R. F. Katz (2006), A semi-Lagrangian Crank-Nicolson algorithm for the numerical solution of advection-diffusion problems, *Geochim. Geophys. Geosyst.*, 7, Q04014, doi:10.1029/2005GC001073.
- Staniforth, A., and J. Côté (1991), Semi-Lagrangian integration schemes for atmospheric models—A review, *Mon. Weather Rev.*, 119(9), 2206–2223.
- Stock, J. D., and D. R. Montgomery (1999), Geologic constraints on bedrock river incision using the stream power law, *J. Geophys. Res.*, 104(B3), 4983–4994.
- Tucker, G. E., and K. X. Whipple (2002), Topographic outcomes predicted by stream erosion models: Sensitivity analysis and intermodel comparison, *J. Geophys. Res.*, 107(B9), 2179, doi:10.1029/2001JB000162.
- Tucker, G. E. (2004), Drainage basin sensitivity to tectonic and climatic forcing: Implications of a stochastic model for the role of entrainment and erosion thresholds, *Earth Surf. Process. Landforms*, 29, 185–205, doi:10.1002/esp.1020.
- Tucker, G. E., and G. R. Hancock (2010), Modelling landscape evolution, *Earth Surf. Process. Landforms*, 35, 28–50, doi:10.1002/esp.1952.
- Turowski, J. M., D. Lague, and N. Hovius (2007), Cover effect in bedrock abrasion: A new derivation and its implications for the modeling of bedrock channel morphology, *J. Geophys. Res.*, 112, F04006, doi:10.1029/2006JF000697.
- Turowski, J. M., D. Lague, and N. Hovius (2009), Response of bedrock channel width to tectonic forcing: Insights from a numerical model, theoretical considerations, and comparison with field data, *J. Geophys. Res.*, 114, F03016, doi:10.1029/2008JF001133.
- van der Beek, P., and P. Bishop (2003), Cenozoic river profile development in the upper Lachlan catchment (SE Australia) as a test of quantitative fluvial incision models, *J. Geophys. Res.*, 108, 2309, doi:10.1029/2002JB002125.
- Weissel, J.K., and M.A. Seidl (1998), Inland propagation of erosional escarpments and river profile evolution across the southeast Australian passive continental margin, in *Rivers Over Rock: Fluvial Processes in Bedrock Channels*, edited by K.J. Tinkler, and E.E. Wohl, pp. 189–206, American Geophysical Union Geophysical Monograph 107, Washington, D.C.
- Whipple, K. X. (2001), Fluvial landscape response time: How plausible is steady-state denudation? *Am. J. Sci.*, 301(4/5), 313–325.
- Whipple, K. X. (2004), Bedrock rivers and the geomorphology of active orogens, *Annu. Rev. Earth Planet. Sci.*, 32(1), 151–185, doi:10.1146/annurev.earth.32.101802.120356.
- Whipple, K. X., and G. E. Tucker (1999), Dynamics of the stream-power river incision model: Implications for height limits of mountain ranges, landscape response timescales, and research needs, *J. Geophys. Res.*, 104(B8), 17661–17674.
- Whipple, K. X., and G. E. Tucker (2002), Implications of sediment-flux-dependent river incision models for landscape evolution, *J. Geophys. Res.*, 107(B2), doi:10.1029/2000JB000044.
- Whipple, K. X., G. S. Hancock, and R. S. Anderson (2000), River incision into bedrock: Mechanics and relative efficacy of plucking, abrasion, and cavitation, *Geol. Soc. Am. Bull.*, 112, 490–503.
- Whittaker, A. C., P. A. Cowie, M. Attal, G. E. Tucker, and G. P. Roberts (2007a), Bedrock channel adjustment to tectonic forcing: Implications for predicting river incision rates, *Geology*, 35(2), 103–106, doi:10.1130/G23106A.1.
- Whittaker, A. C., P. A. Cowie, M. Attal, G. E. Tucker, and G. P. Roberts (2007b), Contrasting transient and steady-state rivers crossing active normal faults: New field observations from the Central Apennines, Italy, *Basin Res.*, 19(4), 529–556, doi:10.1111/j.1365-2117.2007.00337.